Equine Endometrial Development: Setting the Stage for Reproductive Success

by

Natalie Stefania Fraser

A thesis submitted to the Graduate Faculty of
Auburn University
in partial fulfillment of the
requirements for the Degree of
Master of Science

Auburn, Alabama
December 12, 2015

Keywords: uterine development, multispectral imaging, digital image processing, horse, progesterone receptor, estrogen receptor

Approved by

Robyn R. Wilborn, Chair, Associate Professor of Clinical Sciences
Aime K. Johnson, Associate Professor of Clinical Sciences
Timothy D. Braden, Associate Professor of Anatomy, Physiology and Pharmacology
Frank F. Bartol, Alumni Professor of Anatomy, Physiology and Pharmacology

Abstract

Uterine development in the foal is initiated prenatally; endometrial adenogenesis, or gland development, is initiated in the fetus and completed postnatally. To date, there is little data describing this process in the horse. The objective of this study was to characterize uterine development in normal foals and to provide a systematic assessment of equine uterine endometrial development during fetal and neonatal periods. Uterine tissue was acquired from a total of 38 foals of varying ages, ranging from gestational day (GD) 300 to postnatal day (PND) 180. Twenty-eight of the 38 original tissue samples were snap-frozen in optimum cutting temperature (OCT) gel and sectioned at 6µm. Tissue sections were processed for immunofluorescent analysis of estrogen receptor, glucocorticoid receptor, and Ki-67 in situ. Additional tissue samples were stored in Universal Molecular Fixative (UM) for immunohistochemical evaluation of progesterone receptor expression, and for assessment of endometrial histogenesis.

Histological evaluation revealed that nascent endometrial glands were present in all perinatal samples, consistent with previous descriptions. Labeling index (LI), indicative of cell proliferation, was calculated as a percentage of cells expressing Ki67 for each endometrial cell compartment including luminal epithelium (LE), glandular epithelium (GE) and stroma (ST). Overall, main effects of age ($P = 0.005$), cell compartment (GE, LE, ST; $P < 0.0001$) and an age by cell compartment interaction ($P < 0.0001$) were identified for Ki67 labeling index. Consistent with observations based on

results of immunohistochemistry (IHC) studies, Ki67 LI increased ($P < 0.0001$) from the prenatal to the postnatal period, and was higher overall ($P < 0.0001$) in epithelium (GE and LE) versus ST. Postnatally, Ki67 LI increased ($P < 0.0001$) from week 1 to week 24. Progesterone receptor (PR) was observed in LE, GE, and ST at all ages. Overall, a main effect of cell compartment (GE, LE; $P < 0.0001$) and an age by cell compartment interaction ($P = 0.01$) were identified for PR labeling index. Consistent with observations based on results of IHC studies, PR LI was higher in GE than LE for all age groups.

Results indicate that during late fetal and early neonatal life, equine endometrium demonstrated a low degree of proliferation, as defined by a low Ki67 LI. This is in contrast to other species where proliferation is rapid in early neonatal life. This may indicate that endometrial development in the horse is a less organized event during the time periods evaluated relative to other species. Results also demonstrate that multi-spectral imaging is a valuable analytical methodology that can be used in equine tissues.

Acknowledgments

- Thank you to the Birmingham Racing Commission for their financial support
- Thanks to my advisor, Dr. Robyn Wilborn, for her guidance and patience during my residency as well as the rest of my committee members (Dr. Johnson, Dr. Braden, and Dr. Bartol) for their time and advice.
- Thanks to Ms. Anne Wiley for her countless hours in the lab teaching, and Ms. Meghan Davolt and Ms. Dori Miller for all their technical and moral support
- Thank you to Dr. Igor Canisso and Dr. Laura Kennedy for assistance in acquiring tissues for this study.
- Thanks to my resident mates, Dr. Chance Armstrong, Dr. Jennifer Koziol, and Dr. Rochelle Jensen for their constant support and coffee delivery.
- Much gratitude is due to my husband, Brandon, for all his support, post cards, long distance phone calls, and airplane tickets.

Table of Contents

List of Tables

List of Illustrations

List of Appendices

List of Nomenclature

LE	Luminal Epithelium
GE	Glandular Epithelium
E2	17β-Estradiol
P4	Progesterone
UM	Universal Molecular Fixative
ER	Estrogen Receptor
ESR1	Estrogen Receptor-α
ESR2	Estrogen Receptor-β
PR	Progesterone Receptor
GR	Glucocorticoid Receptor
IRS	Immunoreactive Score
IHC	Immunohistochemistry
LI	Labeling Index
PGF	Prostaglandin(s)
PGF2α	Prostaglandin F2α
PGE1	Prostaglandin E1
PGE2	Prostaglandin E2
eCG	Equine Chorionic Gonadotropin
hCG	Human Chorionic Gonadotropin

GnRH	Gonadotropin Releasing Hormone
LH	Luteinizing Hormone
Sv	Endometrial Surface Gland Density
INF-τ	Interferon Tau
PMD	Paramesonephric Duct
FRT	Female Reproductive Tract
UGKO	Uterine Gland Knockout Model
ICI	ICI 182,780
MPA	Medroxyprogesterone Acetate
PCNA	Proliferating Cell Nuclear Antigen
EV	Estradiol Valerate
OCT	Optimal Cutting Temperature compound
UM	Tissue-Tek Xpress™ Universal Molecular Fixative
DBD	DNA binding domain
LBD	Ligand binding domain
AR	Androgen Receptor
MR	Mineralocorticoid Receptor
ERKO	Estrogen Receptor Knockout
PRAKO	Progesterone Receptor Isoform A Knockout
PRBKO	Progesterone Receptor Isoform B Knockout
GD	Gestational Day

PND	Postnatal Day
SC	Stratum compactum
SS	Stratum spongiosum
ST	Stroma
MYO	Myometrium
PERI	Perimetrium
MSI	Multi-Spectral Imaging
DIP	Digital Image Processing
CP	CellProfiler™
CPA	CellProfiler™ Analyst
PMD	Paramesonephric ducts
WNT4	Wingless Type MMTV integration site family, member 4
RSPO1	R-Spondin 1
FOXL2	Forkheadbox L2
PAX2	Paired-box gene 2
LIM1	LIM Homeobox 1
SR	Steroid receptor
Mab	Monoclonal Antibody
PBS	Phosphate buffered saline
NGS	Normal Goat Serum
DAPI	4’,6-diamidino-2-phenylindole

BF	10% (V/V) neutral buffered formalin

I. Literature Review

1.1 Reproductive Physiology of the Equine Endometrium

Equids are seasonally polyestrous, exhibiting repetitive reproductive cycles at approximately 21 day intervals throughout the physiologic breeding season of the spring and summer months. Cyclicity is associated with increasing day length, with the natural ovulatory period spanning from May to October in the Northern hemisphere (1). The estrous cycle of the mare is divided into two phases: estrus, which is the period of sexual receptivity to the stallion, and diestrus, which is the period of nonreceptivity. Of the approximate 21 day estrous cycle, the length of diestrus is relatively fixed at 14 to 15 days, with estrus averaging 7 days in length but having considerably more individual variability between mares. Characteristic behaviors associated with estrus and diestrus in the mare are influenced by the dominant structures on the ovary for the given phase of the cycle, namely the production of estrogen (17β-estradiol) by the dominant follicle during estrus, and the production of progesterone by the corpus luteum during diestrus. In addition to changes associated with ovarian structures, the endometrium of the mare undergoes characteristic physiologic changes associated with stages of the estrous cycle.

Equine endometrial histology was first characterized by Seaborne in 1925 by assessing reproductive tracts from 19 adult mares at the time of slaughter (2). Histologically, the equine uterus consists of the mucosa or endometrium, myometrium (MYO), and perimetrium (PERI). The endometrium can be further classified histologically into epithelial and stromal (ST) compartments. The former includes both

luminal (LE) and glandular epithelium (GE), while the latter includes both dense (stratum compactum), and more loosely organized (stratum spongiosum) stromal zones. Since these initial structural surveys were established, assessment of endometrial histology has become an important tool in the clinical management of broodmares as a means of diagnosing disease and predicting future fertility. The framework for evaluating endometrial biopsies was established by Brandt, Kenney (3), and Rickets (4). The current system of endometrial biopsy assessment is the four category system modified by Kenney and Doig in 1986 (5). This system semi-quantitatively assesses multiple areas of endometrial health, including the presence of inflammatory cells, abnormalities of the endometrial glands (periglandular fibrosis, cystic glands), and presence of normal vascular and lymphatic structures. Endometrial biopsy grading has become a topic of extensive review due to its impact on the broodmare industry (6-9).

1.1.1 Endometrial Changes Associated with the Estrous Cycle

In addition to behavioral changes, steroid hormones affect both gross and histologic changes in the endometrium. Grossly, the presence of 17β-estradiol (E2) results in increased vascular permeability of endometrial tissues with subsequent endometrial edema (10, 11). Characterization of the progression and regression of endometrial edema is used as aid in breeding management programs, where endometrial edema continues to increase in intensity concurrent with the growth of the dominant follicle, and begins to regress just prior to ovulation. Endometrial edema results in endometrial glands appearing straighter and less numerous per unit of endometrial area when compared to the condition seen during diestrus (3, 12). Conversely, progesterone (P4) is responsible for causing substantial uterine and cervical tone and subsequent

quiescence to prepare for the presence of a conceptus, as well as a total lack of endometrial edema during the period of P4 dominance (10). The endometrial glands become more branched and coiled under the influence of P4 during diestrus (3, 5, 12).

Although there may be some effect of breed on endometrial architecture, the essential morphology of the endometrium is similar between Welsh Pony and Thoroughbred mares, with the same physiologic changes occurring in both groups relative to stage of estrous cycle (12). Britton (13) evaluated endometrial biopsies and cytology samples from seven mares from early spring through late autumn; the author reported no obvious change in endometrial architecture related to time of year during the physiological breeding season,

On a microscopic level, sex steroid hormones regulate both endometrial growth and differentiation, as well as steroid receptor concentrations within the equine endometrium (14). Previous studies showed that estrogen receptors (ER) and progesterone receptors (PR) are found in uterine cell nuclei in the mare, as reported for other species (14, 15). Previous studies by Watson and Aupperle (15) employed immunohistochemistry for qualitative assessment of receptor distributions *in situ*. Aupperle observed expression of endometrial ER and PR was related to peripheral plasma hormone concentrations, and that rising plasma E2 concentrations occurred at the same time as synchronous expression of ER and PR and proliferation of stroma cells (15). Cell proliferation was quantified in this study by estimating the number of cells positively labeled for Ki67, and ER and PR expression intensity was calculated using an immunoreactive score (IRS) that was adapted from a method of evaluating ER in human

breast carcinomas. The IRS included the following factors: user-defined staining index and intensity values, percentage of labeled cells, and a weight factor.

Watson used a subjective scale, where staining characteristics were rated from zero (no staining) to three (maximum staining). Visual assessment indicated that in estrus, PR was strongest in the stroma as compared to either LE or GE, with weak staining in the myometrium. Immunostaining for ER was strongest in the stroma, less intense in GE, and weak in LE. In diestrus, the overall intensity of staining for PR and ER was decreased in both the myometrium and stroma (14). In contrast, Aupperle et al (15) concluded that rising E2 during estrus resulted in the synchronous expression of endometrial ER and PR, and proliferation of stromal cells measured by Ki67 labeling index. In early diestrus, as plasma progesterone (P4) rose and plasma E2 levels decreased, peak Ki67 expression occurred in GE. (15). Cell proliferation measured by Ki67 expression, was low in LE throughout the estrous cycle. Based on their results, Aupperle and colleagues recommended dividing equine endometrial proliferation into two distinct phases including: 1. stromal proliferation occurring just prior to and during early estrus; and 2. epithelial proliferation (specifically GE) occurring during early diestrus (15). Differences in descriptive results reported by Watson and Aupperle in different publications (14, 15) in this area are likely related to the inherently subjective assessment of staining intensity using standard IHC methods. Both authors agreed that ER expression was low in GE/LE compared to ST; Watson described a decrease in PR intensity in ST/MYO relative to GE/LE, whereas Aupperle described an increase in PR expression in GE during diestrus.

Lefranc and colleagues described the morphology of endometrial glands during early pregnancy in mares, including calculation of endometrial gland surface density (Sv) defined as the surface area per unit volume of endometrial glands in the *stratum spongiosum* (SS) (16). Endometrial gland surface density was calculated from computer assisted morphometric assessments where uniformly random linear probes were overlaid on vertical sections of SS; a computer calculated Sv based on the number of intersection points between the linear probes and the boundaries of the endometrial glands. No differences in endometrial gland morphology or Sv were observed between pregnant and non-pregnant mares on day 12 post-ovulation, or between the gravid and nongravid horns in pregnant mares at days 20, 25, and 30 of gestation. The Sv endometrial glands increased as gestation advanced (16). A temporary decrease in Sv was noted at day 16, which is the period of embryonic fixation. The authors hypothesized this occurred due to local stromal edema beneath the conceptus at that time. A hypothetical mechanism proposed by the authors was that estrogens produced by the conceptus resulted in localized edema and increased vascular permeability at the time of fixation and subsequent attachment.

Chavette-Palmer and colleagues evaluated steroid receptor populations in the uterus of mid- to late gestation mares from GD 150 to term via receptor binding assays (17). Uterine pieces (volume= one cm^3) were snap-frozen and ground in a mortar under liquid nitrogen; the tissues were homogenized and ultracentrifuged. The supernatant (cytosolic fraction) was stored separately from nuclear extracts, and only the cytosolic fraction was analyzed. In mid to late gestation mare uteri, there was no difference in ER, PR, or glucocorticoid receptor (GR) concentration with increasing gestational age as

measured via radioreceptor assay of the cytosolic fraction (17). Total uterine ER concentration was higher in pregnant as compared to nonpregnant mares, but no difference was noted in total uterine glucocorticoid receptor concentrations between pregnant and nonpregnant mares, or among groups of pregnant mares. Taken together, data were interpreted to suggest that the equine uterus may be very sensitive to the actions of estrogens during pregnancy (17).

1.1.2 Maternal-Conceptus Interactions

Similar to other mammals, there are several complex and orchestrated events that occur between the uterus of the mare and the developing embryo that are necessary for a successful pregnancy. After fertilization, the equine embryo continues development within the oviduct for approximately 6 days (18). At approximately day 4 post-fertilization, the compact morula stage embryo begins secretion of prostaglandin E2 (PGE2), suspected to be responsible for allowing the relaxation of the ampullary-isthmic sphincter and continued progression of the embryo towards the oviductal papilla (18). Similarly, it is PGE2 secretion by the embryo which is suspected to be responsible for relaxation of the oviductal papilla, which is an anatomical feature unique to the mare. Unfertilized oocytes do not routinely pass into the uterus due to lack of secretion of these compounds.

The phrase “maternal recognition of pregnancy” was first coined by Short in 1969 (19) to describe the series of events occurring between the conceptus and uterus in order to prevent luteolysis and continue maintaining the uterus in a progestational state. In species other than the mare, specific compounds have been identified as secreted by the developing conceptus as an aid in signaling maternal recognition of pregnancy, such

as interferon tau (INF-τ) in ruminants or embryonic estrogens in pigs (20). In ruminants, prostaglandins and lysophospholipids also support maternal recognition of pregnancy (21). Secretion of INF-τ results in luteostasis and continued maintenance of the pregnancy; lysophospholipids, other arachidonic acid derivatives, and prostaglandins assist this mechanism.

To date, no single compound or group of compounds has been identified to be responsible for maternal recognition of pregnancy in the horse. In stark contrast to other commonly studied domestic species, the equine embryo is surrounded by a glycocalyx (the embryonic capsule) that maintains the spherical shape of the conceptus, between days 10-16 post ovulation. The equine embryo hatches from the zona pellucida on approximately day seven post ovulation to remain surrounded by the capsule until the third week of gestation (22). The equine embryo remains unattached to the endometrium, and moves continuously throughout the uterus during this period. This movement is thought to be necessary for maternal recognition of pregnancy in mares, as experimental reduction in endometrial contact with the migrating conceptus results in pregnancy loss in mares (23). Estrogen receptor-α (ESR1) is downregulated in the endometrium of pregnant mares versus nonpregnant mares (24). Such downregulation was reported by others (25) to be associated with the down regulation of prostaglandin (PGF) synthesis during maternal recognition of pregnancy through disruption of oxytocin receptors in the endometrium (20, 24).

The unique structure of the blastocyst capsule has an important function in embryonic survival. The negative electrostatic charge of the glycocalyx capsule results in attraction of proteins found in uterine glandular secretions, or histotroph (18). These

secretions are essential for survival of the embryo for the first 40 days of gestation (26). Thus, endometrial glands play a pivotal role in the survival of the conceptus.

One of the unique aspects of reproductive function in the mare is the formation, function, maintenance, and sloughing of the endometrial cups. The cups are distinct, raised areas that form at the base of the pregnant uterine horn. A strip of specialized trophoblastic cells appear at the margin of the yolk sac and the chorioallantois forming the so-called chorionic girdle. The trophoblastic cells of the chorionic girdle invade the endometrium to form the cells of the cups which secrete equine chorionic gonadotropin (eCG); thus, endometrial cups and the chorionic girdle demonstrate a unique conceptus-endometrial interaction that is specific to equids, and that is required for maintenance of pregnancy. Formation of endometrial cups is vital to pregnancy maintenance in the mare, as subsequent production of eCG results in formation of accessory corpora lutea. Chorionic gonadotropins are produced only by equids and certain primate species (27, 28), which allows the mare to be a model for trophoblast-endometrial interactions with implications on human health. Phenotypic similarities between the human and horse placenta include conservation of the basic cell types and essential properties, although some functions were distributed differently (29). Each principle type of equine trophoblast cell has a human counterpart. Equine allantochorion trophoblasts correspond to the human villous cytotrophoblasts; both have stem cell-like properties that allow differentiation into other trophoblast types (29). Their function differs in that in the equid, this cell type is a primary mediator of nutrient exchange whereas this is a function of the syncytiotrophoblast layer in humans. The chorionic girdle trophoblasts of the mare are analogous to human extravillous

trophoblasts; both cell types are invasive and migrate into the endometrial stroma (29). Last, equids and humans both have a multi-nucleate, terminally differentiated cell type- the equine endometrial cup trophoblasts and human syncytiotrophoblasts (29). The endometrial cups also aid in immunologic tolerance of the fetus within the uterus of the mare, as the fetus is a type of allograft (29-32). The trophoblast cells at the endometrial cup interface do not express either MHC class I or MHC class II antigens (33-35), and thus do not pose an immunological challenge to the mare (31).

The endometrial cups are grossly visible as a circle or horseshoe of endometrial protuberances around the conceptus in the gravid uterine horn in dissected embryos. The cups measure 1–2 cm in width but they can vary considerably in length, and can appear as individual, well-separated structures of only 1–3 cm to elongated ribbons of cup tissue that may be >20 cm in length (26). Endometrial cup formation can be described in distinct phases: attachment, invasion, phagocytosis, migration, and differentiation (1). Prior to attachment, portions of the endometrial epithelium become glycosylated; in this enzymatic process, saccharides are suspected to play a key role in attachment of the chorionic girdle of the conceptus. The mononuclear trophoblastic cells terminally differentiate into binucleate eCG-producing cells which invade the endometrium. The formation of the chorionic girdle begins with the formation of shallow folds around day 25 post ovulation. These structures elongate into villous processes around day 33. As pregnancy progresses, an interdigitation occurs between the elongated cells of the chorionic girdle and corresponding endometrial epithelium. Firm attachment at this stage is only between the chorionic girdle, and no other portion of the embryonic vesicle (1, 22, 36).

Invasion begins to progress at approximately day 38; pseudopodia invade the cytoplasm of the endometrial epithelium rather than the intercellular space. Only a small number of girdle cells undergo the process of invasion, with the remainder undergoing necrosis. Phagocytosis occurs when invading girdle cells engulf the disrupted endometrial epithelial cells. The migratory phase is characterized by penetration of the uterine epithelium basement membrane. The trophoblastic cells travel to the endometrial stroma, migrating down the length of the uterine glands. Once the endometrial stroma is invaded, the trophoblastic cells undergo hypertrophy and differentiation into mature cup cells. The girdle cells have a unique amoeboid appearance which is consistent with their functional capacity for migration, invasion, and phagocytosis (1).

The endometrial cups are grossly visible at day 40, reach maturity between days 50 to 60, and slough from the uterine wall between days 70 to 100. Sloughing is complete by day 130. The cup slowly detaches via necrosis and becomes enclosed in a fold of allantochorion (the allantochorionic pouch). Pouches are typically not identifiable at the time of parturition and placental exam postpartum; this excess tissue is suspected to be resorbed in the majority of mares. The endometrium is restored by migration from the periphery, and is fully restored by day 180-200. The cups form a ring or horseshoe at the base of the gravid uterine horn and provide an indication of the orientation of the embryo at the time of formation (26, 37).

1.1.3 Clinical Applications of Reproductive Hormones in Mares

Reproductive hormones are widely used in the manipulation of estrous cycles in mares, predominantly to facilitate breeding. As the mare exhibits her first postpartum

estrus approximately 10 to 14 days after parturition, any compounds administered to the mare may result in inadvertent exposure of her offspring, particularly through mammary secretions. Drug classes used commonly include gonadotropins, steroid hormones (progestogens and estrogens), and prostaglandins, among others (38).

Human chorionic gonadotropin (hCG) and deslorelin acetate are both used to program ovulation in mares for accurate timing of insemination. Human chorionic gonadotropin exerts luteinizing hormone (LH)-like effects, while deslorelin acts in a manner similar to gonadotropin releasing hormone (GnRH). Buserelin, another GnRH agonist, is used to hasten the first ovulation of the breeding season (39). Progestins are used for suppression of behavioral estrus, hastening the first ovulation of the breeding season, and maintenance of pregnancy (38). When progestins are combined with estrogen, they provide greater suppression of the ovarian follicular wave through negative feedback on the hypothalamic-pituitary-gonadal axis, and can be used for synchronization of estrus in mares (38). Prostaglandin F2α (PGF2α) is used for luteolysis and for subsequent ecbolic effects secondary to myometrial contraction, aiding in evacuation of uterine contents. Prostaglandin E1 (PGE1) is used for cervical ripening, while Prostaglandin E2 (PGE2) is applied topically to the oviduct via laparoscope to hasten oviductal transport of embryos. Oxytocin is also used as an ecbolic agent to prevent or treat intrauterine fluid accumulation. Domperidone and sulpiride are used for their pro-prolactin effects, with clinical use in hastening the first ovulation of the year as well as in treating agalactia in mares (40). The developing foal is at risk of exposure to exogenous hormones either in utero or through the mare's

mammary secretions; this warrants further investigation to establish critical time periods of uterine development in this species.

1.2 Endometrial Adenogenesis

The tubular female reproductive tract is derived from the fusion of the paramesonephric ducts (PMD), also known as the Müllerian ducts, with subsequent regression of the mesonephric, or Wolffian ducts (41). Organogenesis begins prenatally; adult uterine phenotype is determined by the degree of fusion of the PMD, which can be complete, partial, or incomplete. Equids exhibit a bicornuate uterus with a moderate degree of fusion, resulting in a "T" shaped organ with relatively short uterine horns and a longer uterine body. This is in contrast to carnivores and suids, which also have a bicornuate uterus but with a lesser degree of fusion and longer uterine horns (42). Although other female reproductive tract (FRT) structures are differentiated at birth, the uterus must undergo considerable further development and differentiation to attain a fully functional adult phenotype.

It was a long standing belief that FRT development was the "default" developmental pathway. This thought process was advanced largely due to a series of elegant experiments performed by Alfred Jost between 1947 and 1952 (43, 44). Briefly, Jost observed that male rabbit fetuses that were castrated in utero, prior to differentiation of reproductive tissues, developed as phenotypic females. Although it was apparent from these experiments that the testis was integral to development of the male reproductive tract, it was not until much more recently that the "default" developmental pathway theory was challenged. In general, these studies evaluating the molecular basis of FRT development were performed in murine species, with results extrapolated to other

species. It is now known that several factors are integral in driving the development of the FRT, and that this is an active rather than passive process. Equally important, the Jost experiments indicated that development of the FRT is an ovary-independent process, in contrast to development of the male reproductive tract which is driven in a positive feedback loop by testicular expression of SRY and SOX9 (45). Factors actively involved in the development of the female gonad include Wingless Type MMTV integration site family, member 4 (WNT4), R-Spondin 1 (RSPO-1), and ForkheadboxL2 (FOXL2). Although it seems that male sex determination is regulated solely through the SOX9 pathway, female ovarian development appears controlled by at least two mechanisms of SOX9 suppression (46).

Development of the tubular genital tract results from both radial and anterior-posterior patterning, such that embryonic mesoderm that develops into the PMD further differentiates segmentally into the oviducts, uterus, cervix and anterior vagina (47). Gene expression coding for transcription factors *Pax2*, *Lim1*, and *Emx2*, as well as the morphoregulatory glycoprotein *Wnt* family are required for normal FRT development (47-49). *Pax2*-null mice experience PMD degeneration during embryogenesis and die soon after birth; thus the underlying tissue basis for development of the kidney and FRT is absent (50). *Lim1* null mice fail to develop oviducts, uterus, or anterior vagina and also lack mesonephric duct derivatives in males (48, 49). Loss of *Lim1* blocks PMD elongation and results in uterine hypoplasia characterized by all cell types in the endometrium (51). *Emx2*-null mice fail to develop reproductive tracts, gonads and kidneys (52)

Several *Wnt* genes play a role in the structure and function of the FRT, including *Wnt4, Wnt5a, and Wnt7a* (53-62). The *Wnt* family is critical in directing epithelial-mesenchymal interactions that drive postnatal uterine development. The *Wnt* family of genes classically acts through a canonical signaling pathway via frizzle receptors (beta-catenin pathway), but can also act through a non-canonical (calcium) pathway. *Wnt5a* is expressed in uterine, cervical and vaginal stroma (53, 59), and *Wnt4* is also expressed in the stroma. In contrast, *Wnt7a* is expressed uniquely by luminal epithelial cells. *Wnt7a*-null mutant mice have a uterus with stratified epithelium rather than columnar, and a small stromal layer that does not contain uterine glands (55). Experiments comparing wild-type to *Wnt7a*-null mutant uteri showed that *Wnt7a* is a potent suppressor of cell death (55). Taken together, these glycoproteins are expressed in specific cell compartments and play unique roles in regional development of the PMD. Tissue recombination experiments showed that epithelially expressed *Wnt7a* and stromally expressed *Wnt5a* are required for uterine gland genesis (58).

In addition to *Wnt* family genes, abdominal-B *Hoxa* cluster genes also play substantial roles in patterning of the FRT. Functional interactions between *Wnt* and *Hoxa* genes have been proposed such that both gene classes work interdependently in uterine development. *Hoxa9, Hoxa10, Hoxa11,* and *Hoxa13* are expressed segmentally along the anterior-posterior axis of the developing PMD; this 'Hox code' directs epithelial and stromal relationships unique to each segment of the developing PMD (oviduct, uterus, cervix, anterior vagina) (47, 63, 64). Restricted, overlapping expression of these genes results in segmental development; *Hoxa9* is expressed in the oviduct, *Hoxa10* and *Hoxa11* are expressed in the uterus, and *Hoxa 11* and *Hoxa 13* are expressed in the cervix

and anterior vagina. This spatially-restricted expression is required to define tissue boundaries (65). *Wnt7a* appears to have a stabilizing effect on *Hoxa10 & 11* stromal expression in the uterus as it is required to maintain (but not induce) stromal expression of these genes (53); this in turn ensures stromal expression of *Wnt4* and *Wnt5a* in the developing uterus (47). In *Wnt7a* knockout mice, postnatal loss of *Hoxa10* and *Hoxa11* expression occurs, revealing that *Wnt7a* is not required for early *Hoxa* gene expression, but is required for maintenance of expression (60).

Despite the obvious importance of normal uterine development, current knowledge of this process in equids is limited. Acknowledging limitations of sample size, Gerstenberg and Allen (51) evaluated endometrial tissue for gland structure and development during the period from 150 days of gestation to 50 days postnatal, and again from nine months of age to 23 months of age. Another report indicated that exogenous estrogen administration from postnatal day 1 through 6 months of age stimulated precocious uterine gland development in the horse (66). Obviously, there are significant gaps in knowledge pertaining to equine uterine development. Limited data for the mare indicate that nascent uterine glands are present in the fetus after gestational day 250, develop further between 5 days and 7 weeks after birth, and complete differentiation after onset of the first estrus (67). Mechanisms regulating this process remain unclear.

In species other than the horse, where the process of endometrial adenogenesis has been studied more intensely, it is clear that this process involves stromal-epithelial interactions that support tissue remodeling, tissue compartment-specific patterns of cell proliferation and locally regulated patterns of steroid hormone receptor expression in epithelial and stromal compartments of the developing endometrium (68-72). Patterns

defined by these cell behaviors, particularly those associated with cell proliferation and hormone receptor expression, can be used to define critical periods of tissue sensitivity to developmental disruption (73, 74). Such information is entirely lacking for the horse.

Current literature devoted to equine endometrial glands is largely focused on the adult mare uterus. However, it is important not to make assumptions about uterine development during fetal and neonatal life based on what is known about adult animals. Tissues are more plastic in earlier stages of development and it is probable that juvenile cell types do not behave as they would in the adult endometrium. This may explain how hormones and xenobiotics encountered during perinatal life in other species exert lasting organizational effects on uterine development and fertility in adults (75, 76).

1.3 Uterine Gland Knock Out Models

A substantive body of literature provides descriptions of the effects of exogenous steroids and xenobiotics on uterine and endometrial development, as well as subsequent reproductive effects in a variety of mammalian species, including the ewe, cow, sow, and mouse (74, 77-82). Effects of sex steroid hormone exposure in neonates can have far reaching implications both in clinical veterinary practice as well as expanding understanding and knowledge of the mechanisms and downstream effects surrounding abnormalities of reproductive tract development and function.

In the ewe, postnatal endometrial adenogenesis was inhibited by administration of norgestromet (83). Phenotypic abnormalities ranged from complete absence of uterine glands, to shallow invaginations into the stroma, to limited numbers of cystic structures in the stroma (80). Uterine gland knock out (UGKO) ewes demonstrate abnormal estrus cycles, presumably due to failure of normal luteolytic

mechanisms related to endometrial release of PGF2α, in addition to inability to establish and support pregnancy (80). Beef heifers treated with P4/E2 implants postnatally had reduced uterine weight and reduced endometrial gland density; effects were more pronounced when implants were placed earlier in life (47).

Tarleton and colleagues (78) evaluated the effects of estradiol valerate and the antiestrogen ICI 182,780 (ICI) on endometrial development in pigs. Similar to other species, porcine uterine gland development is primarily a postnatal event and ERα is a marker of glandular epithelial differentiation (72, 76). Pigs treated with ICI for 7 or 14 days from birth displayed profound reduction in endometrial gland development compared to control animals as reflected by endometrial histology; effects of ICI were most pronounced by PND 14, when endometrial gland development was dramatically retarded in comparison with tissues obtained from corn oil-treated control gilts of the same age (78). In pigs treated with ICI from 7 to 13 days postnatally, endometrial gland depth was not reduced, but overall endometrial thickness was reduced. Results (78) indicated that endometrial adenogenesis in neonatal gilts is an ER-mediated event.

Cooke and colleagues (74) showed that exposure of neonatal mice to progesterone during a critical developmental window inhibited uterine gland development. Similar to the ewe and sow, normal endometrial development in mice is dependent on ER (72, 76), and administration of P4 antagonizes the effects of E2 on developing endometrium, similar to ewes (83). Several progesterone treatment windows were evaluated in mice, including PND 3–9, 5–9, or 3–7 (59). A critical window for P4 exposure, from PND 3-9, was identified. Progesterone exposure during this neonatal

period produced a UGKO (glandless) adult endometrial phenotype in mice, and animals were profoundly subfertile.

The concept that glandless animals are infertile, or at least subfertile, was assessed as a potential strategy for canine contraception first by Wilborn and colleagues (84) and more recently by Ponchon and colleagues (85). Wilborn et al administered medroxyprogesterone acetate (MPA) or saline control to puppies at 5 days of age, repeating dosing when the animals tripled in body weight at approximately 2.5 weeks of age. Uteri were recovered at seven weeks of age for analysis. Endometrial adenogenesis was evaluated by examining histologic sections for morphologic changes and assessment of proliferating cell nuclear antigen (PCNA) as a marker of cell proliferation. No effect of treatment was identified on gland penetration depth, but MPA did reduce canine endometrial cell proliferation in both glandular and luminal epithelial compartments. Ponchon (85) and colleagues administered MPA as a single dose or placebo control to puppies within 24 hours of birth; bitch puppies were evaluated clinically until puberty, defined as the first estrus. Bitches underwent routine ovariohysterectomy to acquire uterine tissue for macroscopic evaluation and histology. No differences were detected between treatment and control groups with respect to uterine wet weight, the area of endometrium occupied by endometrial glands, or the height of the uterine epithelium, thus the authors concluded there was no effect of MPA treatment in this study.

To date, the UGKO phenotype has not been established in the horse. In other species where either a complete or partial UGKO phenotype was produced (74, 78, 82, 83, 86), the role of endometrial development and its outcome on future fertility is better

understood. A similar research model would be ideal to study the role of endometrial histotroph in embryogenesis and early fetal development in the mare. Fertility and fecundity of female animals is a high priority due to economic concerns in most hoofstock species, and developmental conditions that result in either infertility or subfertility can have an impact on production industries. For example, further study into uterine development in pigs has identified that relaxin is required for normal reproductive tract development and is delivered through a lactocrine mechanism, where bioactive factors are transferred from dam to offspring via colostrum ingestion (87-89). Several reproductive parameters in adult sows have been correlated with decreased colostrum consumption as a piglet, such as increased age at puberty for gilts, reduced number of piglets born alive, reduced litter average, and reduced litter average preweaning growth rate during lactation (90). Understanding endometrial and uterine development can have substantive economic impacts, as well as providing the necessary understanding of normal biology as a basis for understanding mechanisms of disease. Targeted disruption of this process could also be used to reduce fertility in target populations, such as management of wild equids.

Wilsher and colleagues (66) evaluated effects of administration of two hormonal treatments given from birth to six months of age on endometrial development in the equid by examining endometrial biopsies obtained from six month old foals and from the same animals at two years of age. The first treatment group received norgestromet implants along with injectable estradiol valerate (EV) and norgestromet at two week intervals from birth to six months (n=4); the second treatment group received altrenogest daily, and injectable EV/norgestromet at two week intervals. A striking

difference in endometrial architecture was evident between the groups in the post treatment endometrial biopsies recovered at age six months. Considerable degrees of endometrial gland morphogenesis and distribution in the stroma occurred in all 4 fillies treated with norgestromet implants with EV/norgestromet injections, including the 2 that were changed from norgestromet implants to altrenogest at age 2–3 months. Complete absence of gland development or only very rudimentary gland development was observed in both the fillies given altrenogest for 6 months and the untreated control fillies. When endometrial biopsy was repeated at 2 years of age, all fillies from all treatment groups exhibited a similar, normal endometrial phenotype. All animals enrolled in this study were ultimately used as embryo donors for other various projects in adulthood, and similar embryo recovery rates were noted between the three groups. Results (66) indicate that equine endometrium did not respond to progestin treatment with the same lasting effects on developing endometrium such as sheep and mice (74, 83). Equine adenogenesis is initiated prenatally, when the fetus is exposed to high levels of circulating progestins (67); thus, it is logical that equine endometrium would not respond to progestins in the same manner as other species, where this process is both initiated and completed postnatally.

Taken collectively, the information on endometrial development highlights several critical components and common themes. First, normal endometrial adenogenesis can potentially be disrupted by administration of exogenous compounds, which results in an infertile or subfertile adult animal. Second, that disruption of this process has the greatest effect when compounds are administered during key developmental windows, which typically occur before the onset of endometrial

adenogenesis, and are not the same across species. Third, although key species differences were noted in response to various compounds, E2 consistently has a positive feedback effect on endometrial proliferation and development, whether through removal of inhibition of development via the "P4 block" at birth or a positive feedback mechanism for the action of E2 on endometrial development.

1.4 Immunohistochemistry (IHC)

Immunohistochemistry is an analytical methodology with broad applications in both clinical and research settings for antigen detection. It is widely used for the detection of steroid receptor proteins *in situ*. Anatomical, immunological and biochemical techniques are all components of immunohistochemical detection, which relies on the binding of antibodies to form an antigen-antibody complex tied to a marker or reporter of some type that can be visualized (91). Depending upon the protocol, tissue samples can be viewed with either light or fluorescent microscopy, and advances in imaging technology now enable the identification and even quantification of multiple target proteins simultaneously.

Immunohistochemistry is used extensively in human reproductive pathology to study various mammary, uterine, and cervical neoplasias (92-97). In mares, IHC used for identification of steroid hormone receptors, and semi-quantitative assessment of receptor expression patterns associated with different stages of the estrous cycle, are documented (14, 15). Such hormone receptor expression patterns were evaluated in pregnant mares during early (98, 99), mid- and late gestation (17).

1.4.1 Tissue Preparation & Fixation

All histotechniques require that tissues be rapidly and appropriately preserved or 'fixed' to preserve tissue histoarchitecture, and to stabilize biochemical elements of tissues and cells that may be targeted for *in situ* analysis. Perfusion or rinsing of tissues to remove blood will reduce the detection of interfering hematologic antigens. Fixation can chemically crosslink proteins and reduce protein solubility. This can result in the masking of targeted antigens. Fixation protocols must be optimized based on the target application and antigen. After fixation, tissues are embedded to facilitate the cutting of sections, which are then mounted on slides (100). Fixation can be considered a foundation step which will prevent tissue degradation and autolysis so that tissue architecture and cell components can be observed following staining and microscopic evaluation (101).

Formaldehyde and related solutions, such as paraformaldehyde or neutral buffered formalin, are the most common fixatives used for histology/histopathology (102). Its most common form in practical use is as a 10% (v/v) solution (~4% formaldehyde), which is either diluted in water (formalin) or in a buffered solution (neutral buffered formalin) (101). Aqueous formaldehyde has many advantages; it is inexpensive and readily available, it works under a variety of conditions, is stable, functions over a wide range of concentrations, and is usable with almost any tissue (102). Formaldehyde acts as a fixative by cross linking within and between molecules, particularly between side chain amino groups of lysine (101). However, secondary and tertiary structures of proteins are unaffected and can be recovered by heating (antigen retrieval) (103, 104). Despite the popularity of formaldehyde as a fixative, it is

ineffective in protocols requiring extraction of DNA or RNA from tissue samples (101, 105), and it may not be the best fixative choice for preserving antigenicity (104). A variety of newer, "molecular fixatives" were developed to address issues associated with the use of formaldehyde based fixatives. These newer fixatives typically have an alcohol or acetone base with other stabilizing agents. In particular, Universal Molecular FIXative (UM) was found to perform nearly as well as frozen tissue sections for molecular diagnostics (105, 106). This fixative is methanol-based with added polyethylene glycol. Some subtle morphological differences occur in tissue histoarchitecture such as eosinophilia or tissue shrinkage; however, staining characteristics are similar between formaldehyde and molecular fixatives (101, 105). Howat and Wilson (101) reported that different processing and staining protocols, as well as the use of different antibodies, can make it difficult to compare the performance of different fixatives between studies for use in immunohistochemistry protocols (101).

Another tissue processing option that can incorporate tissue fixation and embedding in a single protocol is freezing. Freezing tissue samples for diagnostic or research purposes does have certain advantages over alternate fixation and embedding protocols. In clinical settings, frozen tissue is used for rapid intraoperative histopathology. Frozen tissues can be fixed or left unfixed prior to freezing; if unfixed, there is no risk of antigen masking due to crosslinking from interactions with the fixative. The addition of a freezing medium compound, such as Optimal Cutting Temperature compound (OCT; Sakura Finetek USA, Inc, Torrance, CA), is required to use frozen sections for histology; it preserves the morphology of the tissue and protects it from lyophilization effects associated with freezing in the absence of OCT (107). An

embedding medium and cryoprotectant, OCT is a viscous, clear gel at room temperature that is composed of polyvinyl alcohol, polyethylene glycol and other proprietary ingredients (108). Placing the tissue and this freezing medium into a cryomold and freezing them together produces a block with tissue embedded in the OCT medium, which can be mounted directly onto a chuck for sectioning. Samples can be frozen directly in liquid nitrogen, or in isopentane cooled in liquid nitrogen. When samples are frozen directly in nitrogen, the vapor surrounding the block cools it at a slightly slower rate, thus samples frozen in isopentane may retain a slightly better morphology (107). Specific methods of freezing depend on technical goals and aims (107, 109). Despite its preservation of antigens, tissue samples frozen in OCT are not suitable for all applications, most notably mass spectrometry (108), and typically display poor histomorphological integrity when compared to the same tissues processed for embedding in other media such as Paraplast® or Paraplast® Plus.

1.4.2 Primary Antibody Selection

In IHC, targeted antigens are localized *in situ*. This requires selection of a primary antibody with specificity and avidity for the targeted antigen (110). Immuno-localization of the same antigen can vary in different tissues, even under similar fixation and processing conditions (111).

Primary antibodies can be classified as monoclonal or polyclonal. Monoclonal antibodies (Mab) are antibodies that are produced by a single clone of cells or cell line, and consist of identical antibody molecules that target single antigenic epitopes on targeted molecules. Monoclonal antibodies have a high degree of usefulness in biological diagnostics and research applications as they are highly specific in their

binding, homogeneous, and can be produced in essentially unlimited quantities using hybridomas (100). Monoclonal antibodies may be preferred in applications where targeted antigens are highly expressed. However, if for any reason the antigenic site is altered during an experiment, Mabs might not bind (112). Another important characteristic of Mabs is determined by the structure of variable region of the antibody, such as the class or subclass of heavy and light chains, which will determine the affinity for secondary reagents or secondary antibodies (113). Immunoglobulin classes include IgA, IgG, IgD, IgE, and IgM, differentiated by heavy chain type and the ability to form multiple complexes (100, 113). The selection of primary antibodies from differing immunoglobulin classes allows these antibodies to be combined for multi-label studies (114).

In contrast, polyclonal antibodies are antibody molecules that differ in their epitope binding and complementary region amino acid sequence, but share overall target specificity. The specificity of polyclonal antibodies depends on the combination of many clonal products binding to a number of antigenic sites on the targeted molecule. This allows greater adaptability to small changes in the structure of the antigen due to genetic polymorphism, slight denaturation, or other changes (112). However, this characteristic can also lead to an increase in nonspecific binding. Polyclonal antibodies may be favored in applications where lower antigen expression levels are expected as more antibodies can bind a single protein molecule, enhancing the detection signal. Polyclonal antiserum can be created in a short period of time at relatively low cost compared to monoclonal antibodies, but tend to have greater batch to batch variability (112).

Identifying suitable primary antibodies for use in tissues or species less commonly used as research models can prove challenging, as available antibodies may not be validated for use in that particular species. Once the structural region of the antigen that the antibody is generated against is identified, homology between protein structures can be determined to ascertain the likelihood of the antibody working as desired with the tissue of interest. Despite apparent compatibility, some trial and error may be required to identify suitable primary antibodies for the species of interest.

1.4.3 Secondary Antibody Selection

Selection of the secondary antibody is determined by the specific isotype of the primary antibody as well as by the type of immunodetection desired. Secondary antibodies can be conjugated to substances to allow visualization with either brightfield or fluorescence microscopy for IHC. The secondary antibody is raised against the host species for the primary antibody, and must be generated in a different species from that in which the primary antibody was produced. For example, if the primary antibody is a mouse IgG isotype, the secondary antibody must be anti-mouse, raised in a species other than the mouse. Likewise, the secondary antibody must be directed against the same isotype as the primary antibody. This two-step process involving application and incubation of the primary antibody, followed by application and incubation of the secondary antibody, is referred to as indirect detection. Conversely, the primary antibody can be conjugated to a marker or reporter molecule and applied in a single step (direct detection). Although technically less complex in execution, relatively few primary antibodies are available pre-labeled, which requires researchers to perform the conjugation step themselves (115).

Traditionally with IHC, tissue sections are interrogated for a single, targeted antigen. However, it is possible, with careful selection of primary and secondary antibody combinations and optimization of IHC protocols, to target multiple antigens in a single tissue section. Multispectral imaging (MSI) and subsequent digital image processing (DIP) are tools that enable such protocols, as well as the systematic and objective analysis of images generated from them. This has several advantages, including increased processing efficiency. Importantly, MSI, which facilitates capture of wavelength-specific signals in fluorescently labeled preparation, allows the detection and colocalization of multiples labels within the same tissue section and can allow signals captured *in situ* to be quantified. Colocalization of antigens using IHC alone does not imply that such molecules are biologically related in function (115).

1.5 Multispectral Imaging (MSI)

Multispectral imaging combines imaging and spectroscopy. This enables chromogenic or fluorescent labels of overlapping wavelengths to be resolved to single wavelength data. A major advantage of MSI is that labels that were previously indistinguishable to the human eye can be used together and subsequently digitally separated for analysis (114). While some humans can distinguish as many as 500 levels of gray, the majority of people can only distinguish between approximately 35 levels of gray ranging from black to white (116). While the human eye is relatively poor at ascertaining intensity (levels of gray), it is very good at distinguishing colors. However, no two individuals interpret color precisely the same way due to subtle differences in the arrangement of rods and cones in the retina. This can result in bias in human

interpretation of both color and intensity of that color. Used in combination with modern digital imaging processing (DIP) software, these issues can be overcome.

The British scientist Sir George G. Stokes was the first person to observe that the mineral fluorspar exhibits fluorescence when illuminated with ultraviolet light, and coined the word "fluorescence." He also observed that materials that fluoresce emit light at a longer wavelength than the wavelength of the exciting light, a phenomenon that is known as the Stoke's shift, based on Stoke's law (116). In fluorescence microscopy, the absorption spectrum is defined as the range of excitation wavelengths that will evoke fluorescence, and the emission spectrum is the range of emitted light wavelengths that will be observed. For most materials, the Stoke's Shift is fairly small; therefore, both emission and absorption spectra of simultaneously present dyes may overlap. Signal quality is limited by this, as well as by photo bleaching (117).

Autofluorescence is a natural fluorescent property of most biological materials; this results in unwanted background fluorescence. Autofluorescence may be reduced by using narrow band pass filters; these pass only a limited range of wavelengths of light (116). Ideally, excitation filters should be chosen to match the maximum excitation wavelength of the fluorescence label being used, and the emission filter should match the emission maximum. Specific excitation/emission filter combinations are available for most commonly used fluorescent labels. One complicating factor is that for many fluorescent labels of biological interest, emission spectra may overlap or be obscured by autofluorescence from components of the tissue of interest.

The Nuance™ imaging system (Caliper Life Sciences, Hopkinton, MA) combines hardware and software components for powerful MSI analysis. In brief, a series of images is captured at specific wavelengths. Individually labeled images as well as a negative control image to determine autofluorescence are used to generate spectral emission curves for each target of interest. The series of images that results is referred to as an "image cube", with each image taken at each specific wavelength. The data within the cubes is used to define the individual spectra of both autofluorescence and specific labels. Spectral data are combined into a spectral library which is subsequently used for spectral unmixing of multilabeled images for viewing of specifically labeled targets (116).

MSI is not without limitations, and multilabel techniques require careful selection and compatibility of several primary and label-conjugated secondary antibodies. Difficulties may be encountered in identifying appropriate primary antibodies, potential cross reactivity between both primary and/or secondary antibodies, and ultimately antibody validation. Potential antibody combinations should be tested as both single-labeled and multi-labeled images in the desired tissues prior to proceeding to identify any issues with cross reactivity (115). Photo bleaching during image acquisition can be a concern, since order of wavelength acquisition will affect total illumination time. However, as long as some signal is still detectable, unmixing can be accomplished digitally, and relative intensity losses can be accounted for during quantitation (118).

1.6 Steroid Receptors

All steroid receptors (SRs) are ligand-activated transcription factors with affinity for a specific target hormone. Nuclear receptors are ligand-activated

transcription factors that share a common evolutionary history. The steroid receptor subfamily includes estrogen receptors, glucocorticoid receptors, mineralocorticoid receptor, progesterone receptor and androgen receptors. In all SRs, the activating hormone binds in an internal cavity within a well-conserved ligand binding domain (LBD), resulting in a change in LBD conformation, attract coactivator proteins, and increase transcription of target genes (119). In humans, two phylogenetic classes of SRs have been identified. The first group includes ER, whose endogenous ligands are 18-carbon steroids with an aromatized A-ring and a hydroxyl attached to C3 on the steroid skeleton (120). The second group, non-aromatized steroid receptors, contains androgen receptors (AR), mineralocorticoid receptor (MR), GR and PR (120).

Ligands for the non-aromatized steroid receptors all contain a nonaromatized A-ring, an additional methyl at C19, and typically a ketone at C3. SRs differ in their sensitivity to exogenous substances; many environmental chemicals and xenobiotics have been identified which can bind to ER, with relatively few exogenous substances identified which mind to non-aromatized steroid receptors (120, 121). Subsequently, there is increasing realization that the stereochemistry of ligand binding to nuclear receptors and metabolizing enzymes is far more flexible than previously thought, and the "lock and key" model may not be an adequate description for SRs as previously thought (122). Conserved functional domains of steroid receptors include the NH2-terminal transactivation domain, a DNA binding domain, and C-terminal ligand binding domain, among others (123, 124). These domains are independent, yet interact functionally to result in the varied biological actions of steroid receptors.

Steroid signaling can occur through either genomic ("classical") or nongenomic pathways. Some steroid receptors, including GR and PR, have inactive forms which exist in the cytoplasm of the cell, while ER's inactive form is found in the cell nucleus (124-127). Maintenance of the inactive SR state occurs through the actions of chaperone and co-chaperone proteins, which are nuclear-receptor associated proteins (128). Once bound to ligand, the SR alters its conformation and moves to the nucleus, where it works with coregulators to perform transcriptional actions by binding to regulatory DNA sequences on target genes (124). Steroid receptors can also act though protein-protein interactions, rather than DNA-protein interactions by interacting with other transcription factors, repressing the activity of other transcription factors as is commonly seen with GR (129). Genomic actions of SR require nuclear localization of the receptor, and subsequently there is a time lag of 30-60 minutes before effects are noted (124).

In contrast, nongenomic actions of SRs occur rapidly, within seconds to minutes, and are referred to as non-classical actions; these effects can also be mediated through other compounds such as retinoic acids, vitamin D3, and triiodothyronine (130, 131). Nearly all members of the steroid hormone family, including gonadal hormones and glucocorticoids, can exhibit rapid effects (130). Nongenomic actions occur independent of gene transcription or protein synthesis and involve steroid-induced changes in cytoplasmic or of cell membrane-bound regulatory proteins such as mitogen-activated protein kinases (MAPK), phosphatidylinositol-3-kinase (PI3K) or tyrosine kinase (132). Non-genomic actions can occur as nonreceptor-mediated actions at the plasma

membrane, through membrane-associated receptors (other than the classical steroid receptors) or through membrane-bound classical steroid receptors (124).

1.6.1 Estrogen Receptors

Estrogen receptor-α (ESR1) is a member of the nuclear receptor superfamily. Although commonly associated with reproductive tissues, ESR1 has many functions in both normal and neoplastic tissue growth, modulation of bone remodeling, cardiovascular function, immune function and male reproductive physiology (133). In mammals, two primary subtypes of the estrogen receptor, ESR1 and estrogen receptor-β (ESR2) are recognized. More recently, an additional subtype, G protein-coupled estrogen receptor (GPER), was also recognized; these transmembrane receptors are described as demonstrating rapid or "pregenomic" effects (134). G protein-coupled estrogen receptors function is distinct from classical ERs, but may overlap in some cases (135). Therapeutic interventions aimed ER-mediated processes are a topic of considerable research, given the varied effects of estrogen via its action through these receptor subtypes (136-139).

The essential roles of ER have been confirmed through the development and study of ER knockout (ERKO) mice; mice lacking functional ER display an inability to respond to the proliferative and inflammatory stimulus of estrogen (140). Lubahn and colleagues first generated ERKO mice and reported that adult female animals were infertile, with abnormal sexual behavior, hypoplastic uteri, hyperemic cystic ovaries, and no detectable corpora lutea; adult males had reduced fertility (141, 142). However, prenatal sexual development of the ERKO mice was normal, including development of uterine glands (141).

Estrogen receptors-α and -β are the products of separate genes, *ESR1* and *ESR2*, respectively. In humans, the genes are present on separate chromosomes, locus 6q25.1 and locus 14q23-24.1 (133). In the horse, ESR1 is assigned to chromosome 31 (143). The predominant estrogen receptor subtype present in uterine tissue is ERα (144). This steroid hormone receptor is also expressed in the epididymis, testis, ovary, kidney, and adrenal gland. Signals mediated via ESR2 may modulate ESR1-dependent events in the uterus (144). In human fetal tissue, ESR1 is abundant in the uterus and is expressed at a higher level than ESR2 (145). Uterine epithelium in the neonatal mouse lacks estrogen-binding activity, but is still able to respond to estradiol stimulation with an increased rate of cell proliferation; the fact that the underlying mesenchymal cells express ERα suggested that the stroma mediates the effect of the hormone (146). Tissue recombination studies (147) definitively demonstrated that ER expression in stroma mediated the effects of E2 induced cell proliferation on uterine epithelium.

1.6.2 Progesterone Receptor

Progesterone plays a central role in reproductive events associated with the establishment and maintenance of pregnancy, and exerts its action through PR. The PR exists in two isoforms (PR-A and PR-B), which are differentially spliced products of the same gene and are members of the nuclear receptor superfamily of transcription factors (148-151). The two PR isoforms are produced from the same gene via transcription at two distinct promoters and by translation initiation at two alternative AUG signals (148, 152). The production of these two isoforms is highly conserved between species, and the isoforms only differ from each other in that PR-B contains an additional 165 amino acid chain at the amino terminus of the receptor. This additional amino acid moiety

plays an essential role in identifying target genes that are activated by PR-B, but not PR-A (148). Both forms of PR are ligand activated transcription factors; binding of P4 results in dimerization of ligand-receptor complexes, increased receptor phosphorylation, and ultimately binding of these dimers to promoter regions on target genes(123, 148, 150). PR-A has been shown to inhibit ER, GR, and MR dependent gene activation, likely though competition for common limiting coactivators (153, 154). Rapid effects of P4 have also been described that do not involve genomic pathways, mainly through increases in intracellular kinase activity (123, 155-157).

Mice bearing a PR null mutation (PR-Knockout or PRKO mice) were used to define functions supported by PR-mediated signaling (158-161). Studies showed that PR is essential for normal reproductive functions associated with P4 signaling (148, 156, 158-161). Mice lacking both PR-A and PR-B display multiple reproductive abnormalities, including failure to ovulate, uterine hyperplasia and inflammation, failed uterine implantation, abnormal mammary gland morphogenesis, and abnormal sexual behavior responses to P4 (148, 156). Further studies investigating the roles of specific isoforms in either PR-A knockout mice (PRAKO) or PR-B knockout mice (PRBKO) revealed that PR-A is necessary to elicit P4-dependent responses required for normal fertility in female animals, whereas PR-B is required to support normal proliferation and differentiation of the mammary gland (148).

With regard to uterine changes related to the estrous cycle in adult mice, PR is expressed in epithelial, stromal, and myometrial compartments of the uterus with spatiotemporal expression patterns controlled by E2 (140, 156, 162). Estrogen has dual effects of PR expression in adult mice, decreasing levels in LE while simultaneously

increasing levels in ST and MYO (140). In contrast, progestins inhibit many of the actions of E2 on the uterus including epithelial cell proliferation (72). Bigsby and Cunha (163) evaluated the effects of progestins and glucocorticoids on DNA synthesis in the uteri of neonatal mice and showed that treatment with progesterone in 5 day old mice resulted in decreased cellular proliferation in epithelium, and a transient increase in cell proliferation in stroma.

1.6.3 Glucocorticoid Receptor

Glucocorticoid receptor is also a member of the nuclear receptor superfamily. Several GR isoforms exist, which result from alternative RNA splicing and translation initiation of the GR transcript. These isoforms may also undergo a variety of transcriptional, post-transcriptional, or post-translational modifications which ultimately alter the stability and/or function of the final protein (127). Glucocorticoids are regulators of a variety of processes in mammals including metabolic homeostasis, cell proliferation, inflammation, immunity, development, and reproduction (129, 164-166). Cole and colleagues (167) demonstrated that GR knockout mice (GRKO) died shortly after birth due to respiratory failure, with other defects noted including abnormalities in the liver/gluconeogenic pathways and adrenal hypothalamic pituitary axis.

The GR is a ligand-inducible transcription factor; when unbound to ligand, GR resides predominantly in the cytoplasm with a multimeric “chaperone complex” made up of heat shock proteins, immunophilins, and other factors that help prevent degradation of the protein and aid in maturation of the protein (126, 127). Nearly every cell type in the body expresses GR (168), and different transcriptional outcomes are due to tissue-specific expression patterns (164). GR can also alter the physical or chemical

properties of cell membranes, which may support the rapid anti-inflammatory effect seen with glucocorticoid administration (126).

Administration of the synthetic glucocorticoid dexamethasone to rats and mice blocked E2-induced uterine growth and differentiation, leading to diminished rates of embryo implantation (169). Dexamethasone also blocked inflammatory effects of E2 on the endometrium (170). More recently, dexamethasone was shown to inhibit LE proliferation in the neonatal mouse uterus (171). These effects were determined to occur through both PR and non-PR (presumably GR) mechanisms, as dexamethasone inhibited uterine LE proliferation in PR-knockout mice, although to a lesser extent than in wild type mice (171). Taken together, results indicate that glucocorticoids act as estrogen antagonists, and may act synergistically with P4.

In human endometrium, GR is expressed specifically in the stromal compartment (172). Although GR was identified in the uterus of pregnant mares via binding assays, receptor location *in situ* was not determined (17). Presence or absence of GR, or localization to a specific cell compartment has not been evaluated in fetal or neonatal horses.

1.6.4 Proliferation Markers

1.6.4.1 Ki67

Ki67 antigen is a protein that is associated with proliferating cells. It is present in the nuclei of cells in G_1, S and G_2 phases of the cell cycle as well as during mitosis, but is absent in quiescent (G_0 phase) cells (173). Consequently, Ki67 has been used as a marker of proliferating cell populations in both normal and neoplastic tissues. The complete primary structure of Ki67 was published by Schluter and colleagues (174)

in 1993, and The human Ki67 gene and complementary protein were completely sequenced (175). A key regulatory function has yet to be assigned to Ki67. However, the utility of this protein as a marker of cell proliferation is well recognized. In order to consider a protein for use as a proliferation marker, two qualities must be met (176). First, the protein must be continuously present in all active phases of the cell cycle of all cell types. Second, the protein should disappear rapidly in quiescent cells. The Ki67 protein meets these criteria.

Proliferation markers can be used to determine which cells have the potential to divide at some point in the future, but not to actually predict division of the cell (177). This is notable when the growth kinetics of a cell are disrupted by exogenous factors such as drugs. For example, cells may remain Ki67 positive when DNA synthesis is blocked by hydroxyurea, as these cells are arrested in mitosis (178). It is important to remember that cell proliferation is not regulated through a binary process or "on-off" switch, but involves a complex array of factors. Interfering with one part of the proliferative process may not affect all other parts equally, resulting in expression of some proliferation markers in non-dividing cells. Thus, cells that are positively labeled for Ki67 should be interpreted as outside of G_0 or the quiescent phase of the cell cycle with potential to proliferate.

Ki67 is used extensively to monitor the growth fraction of cells, particularly with respect to prognosis of neoplastic tumors (174, 177, 179-187). A labeling index can be calculated by determining the percentage of Ki67 labeled cells in a target cell population (177). The original prototype anti-human Ki67 had limited species cross reactivity for some primates, but not other domestic species (177). A panel of new

monoclonal antibodies against Ki67 was raised and designated *MIB* (for Molecular Immunology Borstel), and this antibody (MIB-1) was used to stain the Ki67 equivalent proteins in various mammals including cattle, dogs, horses and sheep while another variant (MIB-5) had cross reactivity with rodents (177). Therefore it was possible to assess cell proliferation using Ki-67 as a proliferation maker in most mammals used in research.

1.6.4.2 Proliferating Cell Nuclear Antigen

Proliferating cell nuclear antigen (PCNA) is an auxiliary protein of DNA polymerases δ and ε is involved in DNA replication and repair (188). PCNA was initially described as a nuclear antigen, identified in proliferating cells by autoimmune sera obtained from patients with autoimmune disease (189). A protein, PCNA is comprised of 261 amino acids, and has an estimated molecular weight of 29 kDa (188). Since PCNA is associated with both DNA repair and replication, it is less specific for cell proliferation than Ki67.

II. Hypothesis and Objectives

Disruption of the normal developmental program during what Charles Stockard (190) referred to as “critical moments”, or periods of development, can have lasting consequences for form and/or function of tissues later in life. This is well documented for the female reproductive tract, as data from both laboratory and domestic ungulate species indicate that transient disruption of the uterine developmental program can have lasting effects on uterine histoarchitecture, as well as the capacity of adult uterine tissues to support pregnancy (72). For the mammalian uterus, such critical periods of development are typically associated with perinatal life, when tissues are still developmentally plastic and, by consequence, subject to organizational disruption and ‘(re)programming’ (191). Still, these important organizational periods must be defined for each species. Effectively nothing is known about these relationships in the horse.

The hypothesis underlying research described herein is that advancing understanding of basic equine uterine histogenesis and cellular behaviors associated with endometrial development during perinatal life, including delineation of cell proliferation patterns, and temporospatial patterns of targeted steroid hormone receptor proteins *in situ*, will lead to identification of critical periods of organization when the uterus may be susceptible to developmental disruption. Results are expected to provide information required to define critical periods of development when uterine tissues could be sensitive to the organizationally disruptive effects of steroid hormones, related xenobiotics or environmental endocrine disruptors.

Specific aims were to determine: (1) patterns of endometrial histogenesis associated with the onset and progression of uterine gland development; (2) patterns of endometrial cell proliferation as reflected by cell compartment (glandular epithelium, luminal epithelium and stroma) - specific patterns of immunohistochemical labeling for Ki67, a cell proliferation marker; (3) temporospatial patterns of PR, ESR1, and GR expression using IHC.

III. Materials and Methods

3.1 Acquisition of Uterine Tissues

Thirty-eight individual uteri were acquired from one of three sources. Uteri (N = 21) were obtained from normal, healthy animals as part of other terminal experiments performed at the Gluck Equine Research Center at the University of Kentucky, Lexington, KY. Animals were euthanized as per Institutional Animal Care and Use Committee (IACUC) guidelines for the respective project(s) in which animals were enrolled (projects unrelated to this study). The total number uteri from different pre- and postnatal age categories required for this study was insufficient. Consequently, additional sources were identified.

An additional two uteri were obtained from clinical cases at the Auburn University College of Veterinary Medicine, J.T. Vaughn Large Animal Teaching Hospital. These samples came from animals that were euthanized owing to clinical disease unrelated to the reproductive tract. One uterus was recovered from a foal euthanized due to gastrointestinal colic, and the other uterus was recovered from a late gestation fetus where the dam had been euthanized due to gastrointestinal colic. Finally, uteri (N = 16) were obtained from the University of Kentucky Veterinary Diagnostic Laboratory. These uteri were harvested from foals presenting for routine necropsy. Clinical history was acquired from owner-provided records including age and reason for death or euthanasia. Attempts were made to exclude animals with confounding clinical

history (i.e., failure of passive transfer of colostral immunoglobulins, mares receiving exogenous hormones), but this information was not always available.

The 38 uteri obtained as described above came from both pre- and postnatal periods as indicated in Table 1. Tissues were organized into age group categories by week (fetal/ postnatal), with individual animal ages recorded as gestational day (GD) or postnatal day (PND). Careful histological evaluation of tissue sections from each uterus revealed that the integrity of some tissues was suboptimal for objective analytical purposes. Consequently, the total number of useable samples available for analysis in each age group category for each analytical procedure was ultimately reduced as indicated in Table 1.

Table 1: Tissue Samples Available

Application	Week -7 (fetal)	Week 1 (postnatal)	Week 5 (postnatal)	Week 7 (postnatal)	Week 24 (postnatal)
Total Number Collected	**N=7**	**N=12**	**N=13**	**N=4**	**N=2**
Histology *N=33*	**N=6** GD 300 (3) GD 320 (2) GD 337 (1)	**N=8** PND 0 (5) PND 1 (1) PND 2 (1) PND 6 (1)	**N=13** PND 23 (2) PND 25 (1) PND 26 (1) PND 27 (3) PND 28 (3) PND 29 (1) PND 30 (1) PND 32 (1)	**N=4** PND 45 (1) PND 49 (1) PND 50 (1) PND 70 (1)	**N=2** PND 180 (2)
IHC- Ki67 *N=28*	**N=4** GD 300 (2) GD 320 (2)	**N=5** PND 0 (2) PND 1 (1) PND 2 (1) PND 6 (1)	**N=13** PND 23 (2) PND 25 (1) PND 26 (1) PND 27 (3) PND 28 (3) PND 29 (1) PND 30 (1) PND 32 (1)	**N=4** PND 45 (1) PND 49 (1) PND 50 (1) PND 70 (1)	**N=2** PND 180 (2)
IHC- PR *N=10*	**N=0**	**N=4** PND 0 (2) PND 2 (1) PND 6 (1)	**N= 4** PND 27 (1) PND 28 (1) PND 29 (1) PND 32 (1)	**N=2** PND 45 (1) PND 49 (1)	**N=0**

Table 1 outlines the specific number of tissue samples deemed suitable for each application.

3.2 Data Collection

3.2.1 Tissue Processing and Histology

Cross sections of the uterus were acquired from the base of the left, right, or both uterine horns. Each tissue sample was rinsed with normal saline to remove blood and debris. A piece of each sample was then placed in separate labeled conical tubes containing either 10% (V/V) neutral buffered formalin (BF; Scientific, Inc, Morgantown, PA) or Tissue-Tek Xpress™ Universal Molecular Fixative (UM; Sakura Finetek USA, Inc, Torrance, CA) A third piece of each sample embedded in Tissue-Tek® O.C.T. compound (OCT; Sakura Finetek USA, Inc, Torrance, CA) contained within peel-away boxes, was snap frozen in liquid nitrogen for immunohistochemical analysis. Tissues from the Gluck Equine Research Center were harvested and placed in fixatives by a collaborator.

Fixed tissues (BF, UM) were embedded in Paraplast Plus® (Leica Biosystems Richmond, Inc, Richmond, IL) using standard histology techniques. Tissues were sectioned at 6μm, and nonsequential sections were adhered to pretreated glass slides (Superfrost® Plus, VWR International, LLC, Radnor, PA). Tissue sections were stained with hematoxylin to allow observation of basic histoarchitecture. Stained sections were scanned digitally using an Aperio CS2 slide scanner (Leica Biosystems Inc, Buffalo Grove, IL) and digital images were viewed using Spectrum™ software (Version 11.2.0.780, Leica Biosystems Inc, Buffalo Grove, IL) at 20x. Two to five, nonsequential sections were examined for each animal.

Histologic descriptions for each animal were recorded. First, the various tissue layers present were identified, including the: endometrial stratum compactum, stratum

spongiosum, myometrium, and perimetrium. The presence or absence of endometrial folding was also noted. The entire luminal surface was examined for the presence of glandular structures, and their approximate location relative to endometrial folds was noted. Uterine glands were classified developmentally as displaying bud formation, tubulogenesis, coiling and branching, and/or branching, in accordance with categories described by Gray et al (70).

3.2.2 Immunofluorescent Staining

The following primary antibodies were selected for use and tested in the laboratory for compatibility when combined. Antibody specifications are listed in Table 2; antibody combinations as used in the tissue are listed in Table 4. A monoclonal mouse anti-human estrogen receptor clone 1D5 (DAKO Monoclonal Mouse Anti-Human Estrogen Receptor, Glostrup, Denmark) was selected for immunohistochemical staining of ESR1 in equine tissue. According to the product insert, anti-ER 1D5 was produced in BALB/c mice using recombinant estrogen receptor (RER) which has a molecular mass of 67kD (192). This antibody reacts with an antigenic determinant located in the N-terminal domain of ER, but anti-ER, 1D5 does not recognize ESR2 (193). A rabbit anti-human polyclonal progesterone receptor (DAKO Rabbit Anti-Human Progesterone Receptor, Code No. 0098, Glostrup, Denmark) from the purified immunoglobulin fraction of rabbit antiserum was selected for this project. The immunogen was a synthetic peptide from the DNA-binding domain (amino acids 533-547) of human progesterone receptor in an ovalbumin carrier protein. The manufacturer reports that this antibody had similar reactivity to the monoclonal antibody clone PR AT 4.14, reacting with the same part of the progesterone receptor. These two antibodies did not react with ER, GR, or androgen

receptors, but recognized PR from human breast cancer as well as bovine, rabbit, and murine uteri, indicating that this epitope was conserved among these species. The antibodies bound to a site on the intact undenatured PR, but failed to bind to partially degraded steroid-binding form of the receptor, suggesting that the antibody-binding domain is at or near a site sensitive to proteolysis (194). A mouse monoclonal IgG2 anti-glucocorticoid receptor antibody [BuGR2] (ab2768, Abcam, Cambridge, MA) was selected based on recommendation from the manufacturer regarding protein homology (87% homologous between rat and equine). The immunogen was partially purified rat GR, with previously identified species reactivity in the mouse, sheep, rabbit, guinea pig, and humans.

Tissue blocks frozen in OCT gel were sectioned on a cryostat (thickness = 6µm), and sections were transferred to pretreated glass slides (Superfrost® Plus, VWR International, LLC, Radnor, PA). Slides were stored in a manual defrost freezer at -20° C until staining. For staining, slides were dried with warm air for 60 seconds and then fixed in chilled acetone for five minutes. Slides were removed from acetone and allowed to air dry for 10 minutes to permit evaporation of residual acetone. A 1X working concentration of phosphate buffered saline (PBS) by diluting 10X stock solution PBS (Amresco®, Solon, OH) with distilled water, 1 part 10X PBS to 9 parts distilled water. Slides were then washed in two changes of 1X phosphate buffered saline (PBS) for 3 minutes each, and then each section was outlined with a ImmEdge™ hydrophobic barrier pen (Vector Laboratories, Inc, Burlingame, CA). Non-immune goat serum (NGS; 10% v/v in 1X PBS) was used as a blocking agent. With the blocking agent applied, sections were incubated at room temperature in a humidified chamber for 60 minutes. The

blocking agent was rinsed from the sections with two changes of 1X PBS for three minutes each.

Primary antibody cocktails (Table 2) were prepared in the blocking agent (10% v/v NGS in 1X PBS) with specific antibody dilutions as listed in Table 2. Individual antibody cocktails were applied to all sections, excluding the negative control section, and allowed to incubate in a humidified chamber for 60 minutes. The negative control section remained treated with blocking agent during this time. All sections were rinsed in two changes of 1X PBS for three minutes each.

For all immunofluorescent staining procedures, next steps were performed in dim light. Stock solutions of secondary antibodies were centrifuged at 2000G for three minutes to facilitate aspiration of particulate-free antibody. Secondary antibodies corresponding to their primary target antibodies were prepared as a cocktail (Table 3) with dilutions as noted in 10% v/v NGS in 1X PBS. In each case, secondary antibody cocktails were applied to all sections, including negative controls, and allowed to incubate in a dark, humidified chamber for 60 minutes at room temperature. All sections were then rinsed in two changes of 1X PBS for 3 minutes each. Excess PBS was blotted from the sections and a DAPI nuclear stain was applied in a commercially prepared combination stain/mounting medium (VectaShield® Mounting Medium for Fluorescence with DAPI, Vector Laboratories, Inc, Burlingame, CA) for fluorescent imaging. Slides were stored in an opaque, humidified chamber overnight at 4° C for imaging the following day.

For each staining and imaging session, tissue from a single animal (foal 44) was used to generate positive and negative control images. The same control tissue was used for each antibody combination, and only one antibody combination was stained per day.

Table 2: Primary Antibodies

Primary Antibody	Host	Ig Subtype	Manufacturer	Clone	Concentration	Working Dilution
PR	rabbit		Dako	polyclonal	1.2 gm/L	1:100
Ki67	rabbit		Abcam	polyclonal	0.9 mg/mL	1:100
ESR1	mouse	IgG1	Dako	1D5	166 mg/L	1:50
GR	mouse	IgG2	Abcam	BuGR2	1 mg/mL	1:100
CK8 +18	guinea pig		Fitzgerald Industries International	polyclonal	100 uL	1:400

Listed antibodies were used for various immunohistochemical protocol. Corresponding secondary antibodies are listed in Table 3. The anti-PR primary antibody listed above is no longer available commercially.

Table 3: Secondary Antibodies

Secondary Antibody	Host	IgG Subtype	Manufactuerer	Catalog	Concentration	Working Dilution
Alexa Fluor 594	goat	IgG	Life Technologies Invitrogen™	A21121	2 mg/mL	1:400
Alexa Fluor 546	goat	IgG	Life Technologies Invitrogen™	A11074	2 mg/mL	1:400
Alexa Fluor 488	goat	IgG1	Life Technologies Invitrogen™	A21121	2 mg/mL	1:400
Alexa Fluor 488	goat	IgG	Abcam	AB150117	2 mg/mL	1:400

Listed antibodies were used for various immunohistochemical protocols. Corresponding primary antibodies are listed in Table 2.

Table 4: Primary and Secondary Antibody Combinations

Combination	Respective Primary Antibodies	Paired Secondary Antibodies
Combination1	Anti-ESR1, Anti-PR, Anti-CK8	A488 (IgG1), A546, A594
Combination 2	Anti-GR, Anti-PR, Anti-CK8	A488 (IgG), A546, A594
Combination 3	Anti-Ki67, Anti-CK8	A546, A594

Primary antibodies were combined according to compatible host species and immunotype. Two pairs of antibodies (anti-ESR1 & anti-GR; anti-PR & anti-Ki67)were from the same host species and immunotype and, therefore, could not be combined for imaging.

3.2.3 Multispectral Imaging

Fluorescently labeled fetal and neonatal equine endometrial cross-sections were imaged in 15 total sessions using a Nuance FX MSI system (Caliper Life Sciences, Hopkinton, MA) affixed to a Molecular Machines and Industries (MMI, Haslett, MI) CellCut Workstation using a Nikon TE-2000U inverted microscope (Nikon Instruments Inc., Melville, NY). Five sessions were devoted to sections stained with primary antibody combination 1, 2 sessions for antibody combination 2, and 8 sessions for antibody combination 3 (See Table 4, previous section). Individual animals were assigned randomly to an imaging day. Groups were balanced to insure that tissues from the early, mid-, and late stages of development (Table 5) were balanced reasonably across imaging days to minimize technical bias. The positive control section was examined first, with exposure time determined for each imaging session using this reference section. The positive control section subsequently underwent image capture to determine the

presence of targeted signals. The negative control section was imaged next to determine if non-specific binding was present. If signal was not detected in the positive control section, or if nonspecific binding was detected in the negative control section, the imaging session for that day was aborted. Images from antibody combination 3 (Ki67/CK8) were obtained first. Images from the remaining combinations were abandoned due to poor repeatability between sessions.

For each individual animal, three tissue sections were examined. For each section, images were captured from three unique shallow and three unique deep stromal zones (N = 18 images per animal) identified randomly. All images used for analyses were captured at a constant magnification (40X). Shallow zones were defined as adluminal; the luminal epithelium and uterine lumen were identified, and the section was positioned to maximize the number of cells present in the image while still capturing LE, GE (if present), and stroma. Deep zones were defined by identifying the myometrial-stromal interface and positioning the image to exclude the myometrium. Raw images were captured at fixed exposure times, determined from the autoexposure time for the positive control section for each image day, every 10nm throughout the spectral range (420-720nm). This protocol permitted capture of emission wavelength-specific images of fluorescent signals using long-pass emission filter cubes optimized for the specific signals (Table 6; DAPI , A488, A546, and A594; Chroma Technology Corp., Bellows Falls, VT).

Table 5: Allocation of Tissues to Imaging Day

Date	Antibody Combination	Animal ID and Age
4-29-15	Group 3 (Ki67, CK8+18)	18 (PND 28), 35 (GD 300), A (PND 6)
5-22-15	Group 3	5 (PND 27), 23 (PND 70), 31 (PND 30), 33 (PND 0), X (PND 180)
5-29-15	Group 3	9 (PND 23), 19 (PND 28), 25 (PND 28), 26 (GD 320), 43 (PND 0)
6-2-15	Group 3	10 (PND 29), 13 (PND 25), 14 (PND 23), 41 (PND 0), Z (GD 320)
6-3-15	Group 3	1 (PND 49), 21 (PND 26), 17 (PND 32), 34 (GD 337), D (PND 1)
6-9-15	Group 3	2 (PND 50), 4 (PND 45), 20 (PND 27), 32 (PND 0), 44 (PND 2), B (GD 300)
6-19-15	Group 3	6 (PND 27), 30 (GD 300), Y (PND 180)

Table 5 demonstrates the groups of individual animals for each imaging session.

Table 6: Filter Cube Sets

Cube Description	Excitation Filter (nm)	Emission Filter (nm)
ET 405/20x, T425lpxr, ET460lp	395-415	460 LP
ET 480/40x, T510lprxt, ET520lp	460-500	510 LP
ET 545/25x, T565lpxr, ET575lp	520-570	565 LP

Three filter cubes were used to selectively excite and allow emission of fluorescently-labeled secondary antibodies.

3.2.4 Immunohistochemical Staining

Immunohistochemistry using DAB as a reporter was attempted using anti-PR, anti-ESR1, and anti-GR primary antibodies as outlined in table 2. Acceptable, consistent staining patterns were obtained only with anti-PR. Consequently, further in situ analyses of GR and ESR1 were not pursued. Tissues fixed in UM were embedded in Paraplast Plus®, sectioned (6 µm), placed on coated glass slides, and stored for batch processing on a single date. Tissues from 12 animals (2 sections/animal) were selected for IHC based on tissue integrity.

Tissue sections were deparaffinized in Hemo-De® (Scientific Safety Solvents, Keller, TX) and rehydrated through a graded alcohol series into distilled water. Tissues were then subjected to heat-induced antigen retrieval for 15 min in citrate buffer (pH 6), and allowed to cool at room temperature for 15 minutes. A blocking solution of 10% (v/v) NGS in PBS was applied to all tissue sections at room temperature for 20 minutes. Blocking agent was shaken off all sections prior to application of the primary antibody.

The primary antibody (anti-PR) was diluted in 10% (v/v) NGS and applied to all tissue sections. Slides were placed in a humidified chamber and allowed to incubate at

4°C overnight. The following morning, sections were rinsed in two changes of PBS for three minutes each. Next, hydrogen peroxide (3%, v/v) was applied for 5 minutes to quench endogenous peroxidase activity, and slides were washed in two changes of 1X phosphate buffered saline (PBS) for 3 minutes each. The biotinylated secondary antibody was prepared from a commercially available kit (VECTASTAIN® *Elite* ABC kit, Vector Laboratories, Inc, Burlingame, CA) per manufacturer instructions. One drop of concentrated stock secondary antibody was added to 5 ml PBS containing 10% NGS. The diluted, biotinylated secondary antibody was applied to all tissue sections, which were incubated at room temperature for 40 minutes. Sections were then washed as previously described.

The VECTASTAIN® Elite ABC reagent was prepared by adding two drops of the provided "Reagent A" (proprietary; avidin-biotinylated enzyme complex) to 2.5 ml of PBS with 10% NGS. After mixing, two drops of "Reagent B" (proprietary; enzyme substrate) were added. The mixed reagent was allowed to stand for 30 minutes prior to use and then applied to all sections. Sections were washed as previously described, and 3,3'-diaminobenzidine (DAB) solution was applied to all sections. Sections were examined for adequate color development from DAB application; DAB incubation did not exceed 10 minutes for any section. Sections were washed, dehydrated, cleared, and mounted permanently for image capture.

3.2.5 Digital Image Processing

3.2.5.1 Digital Image Processing of Images Captured using MSI

For image data generated using MSI, a spectral library was built by collecting wavelength-specific data from single labeled tissue sections treated uniquely with anti-

PR, anti-ESR1, anti-GR, anti-CK8 or anti-Ki67 and appropriate secondary antibodies, each selected to produce signal at unique wavelengths (A488, A546 or A594), or that were stained with DAPI alone. Autofluorescence was determined from images that were treated with secondary antibody cocktail alone. In every case, omission of primary antibody resulted in a total lack of fluorescent signal. The resulting image library allowed raw images to be processed based on wavelength-specific target signal corrected for background autofluorescence.

To differentiate between target signals, image data were spectrally unmixed to produce component images based on the established spectral library of emission wavelengths using Nuance FX software (Figure 1). Spectrally unmixed images were comprised of a composite color image containing all target signals, and included individual gray-scale images illustrating individual wavelength data. Data from spectrally unmixed images were exported into CellProfiler™ (CP; open-source software, www.cellprofiler.com) for further analysis.

Cell Profiler™ enabled development of a set of user-defined parameters constructed into an analytical "pipeline" that can be standardized to specific applications. Pipeline modules were developed in order to adjust images for background noise, establish threshold values for signal intensities, delineate cell compartments (EPI from ST, LE from GE), identify cell nuclei, and collect other quantitative measurements objectively. Use of CP enabled generation of properties files which were subsequently exported into CellProfiler™ Analyst (CPA; open-source software, www.cellprofiler.com). The properties files contained configuration information necessary for CPA to access the appropriate data and images for analysis. This enabled

'computer learning.' Because CP was used for the first step in image analysis, properties files were generated automatically as a function of that program.

Random cell nuclei were selected and sorted into appropriate bins to start the CPA computer learning process. After initial cell sorting, CPA was used to generate "rules", which are algorithmic if/then statements, to sort individual cells into two defined populations, Ki67-positive or Ki67-negative. The optimal number of rules used to train CPA was considered a critical parameter, as too few rules results in poor accuracy of the automatic classification scheme. If too many rules were selected, this would result in increased computational time as well as increased time spent training the system. The program user manual (open source; http://www.cellprofiler.org/CPmanual) suggested that 10-50 rules were typically adequate, but this would vary based on the complexity of object appearance and the frequency with which desired objects appeared.

Accuracy of the CPA cell sorting process was assessed in two ways. First, after baseline rules were established, the algorithm was used to identify Ki67-positive or Ki67-negative cell populations. Despite extensive effort using this technology, the algorithm correctly identified and sorted <20% of the cells when a specific Ki67-positive or Ki67-negative cell population was requested. Cross-validation accuracy was also scored by the program, where the program scored the manually sorted training set images using the current rules and compared those results to the actual classification. Based on previously defined laboratory protocols, accuracy was expected to be ≥80%. The program manual recommended a cross-validation accuracy of >80% for two sorting bins, or >95% for three sorting bins. Graphs of cross-validation accuracy are depicted in Figures 2A and

2B. These analyses indicated that cross validation accuracy was approximately 50-60%, which was considered too poor to generate meaningful data using this technology.

Images labeled for Ki67 were examined by hand. All the cells in each image were counted, and a minimum of 1000 total cells (combined LE, GE, and ST) were counted for each animal. Counted cells were classified individually as Ki67-positive (pink) or Ki67-negative (blue) based on color. A labeling index (LI) was calculated by dividing the number of positively labeled cells by the total number of cells counted, and multiplying that value by 100 to determine percent labeled cells.

Figure 1: Multi-Spectral Imaging and Spectral Unmixing

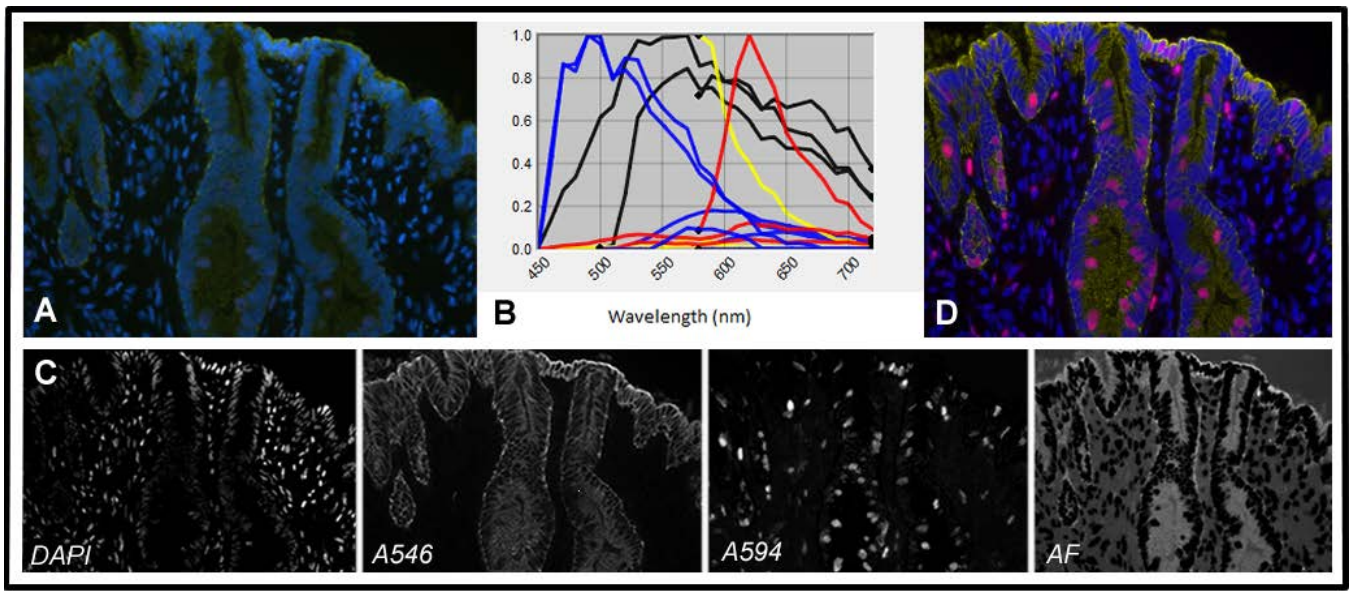

An example series illustrating the spectral unmixing process. First, raw images were acquired (A), and unmixed using a spectral library developed for the unique combination of wavelengths associated with fluorescently-labeled secondary antibodies (B). Spectral unmixing allowed autofluroescence to be substracted (C- AF) as well as extraction of wavelength-specific data for each image (C). An unmixed composite image with data from all wavelengths was the result of this process (D).

Figures 2A & 2B: Cell Profiler Accuracy Determination

2A:

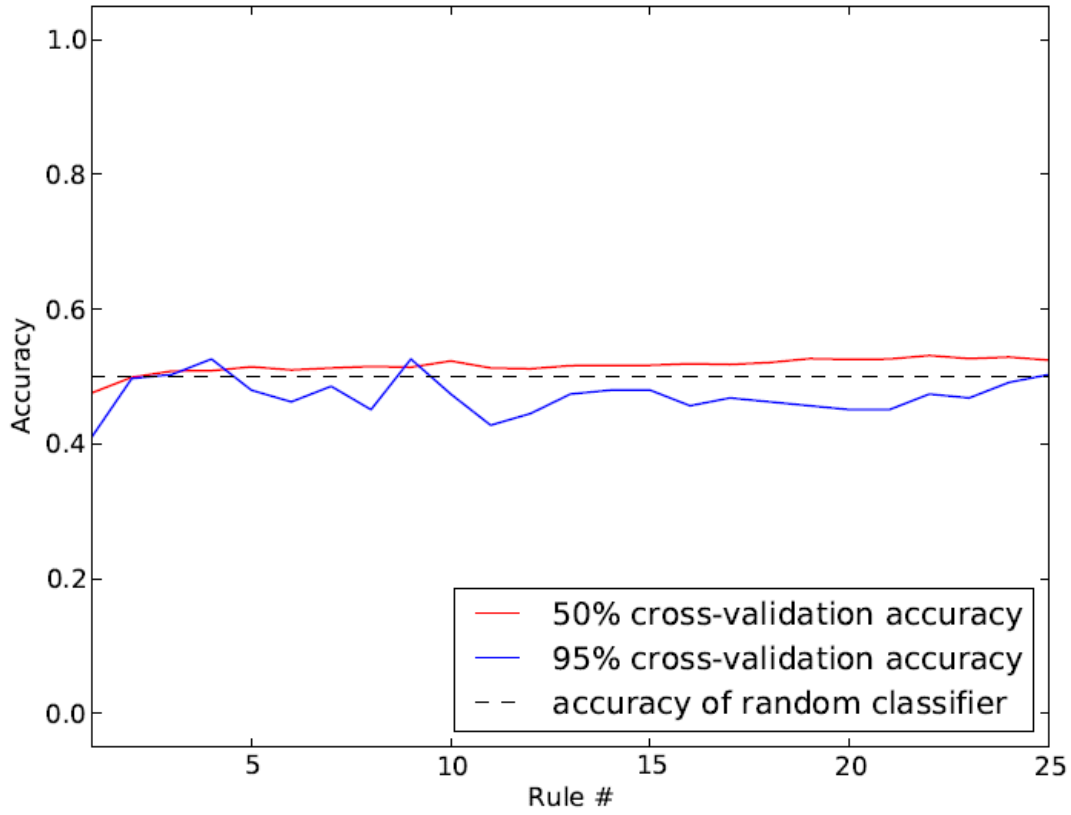

This plot depicts the cross-validation accuracy for the CellProfiler™ pipeline for epithelium. Values closer to 1 indicate better performance. If the accuracy increases (that is, slopes upward) at larger numbers of rules, adding more rules is likely to help improve the classifier; if the line slopes downward, adding further images to the training group may improve accuracy. Second, accuracy is displayed for two versions of cross-validation, with 50% or 95% of the examples used for training and the remainder for testing. If the two accuracies are essentially the same, adding more cells to the training set is unlikely to improve performance.

2B:

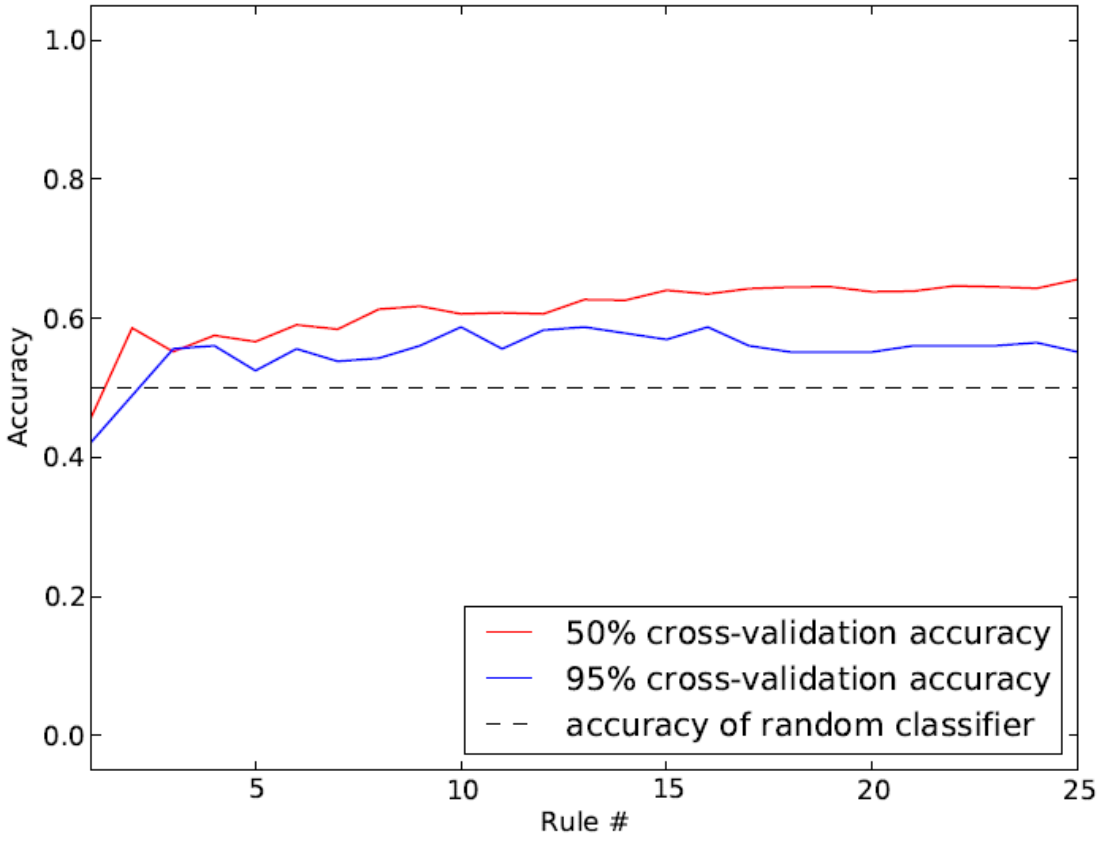

This plot depicts the cross-validation accuracy for the CellProfiler™ pipeline for stromal nuclei. See Figure 2A for description of estimating accuracy. Cross-validation accuracy should be ≥80% for 2 sorting bins, and ≥95% for 3 sorting bins as previously established for laboratory protocols.

3.2.5.2 Digital Image Processing for Standard IHC Targeting of PR

Slides were scanned using an Aperio CS2 slide scanner at 20X to capture digital images. Digital images of 2-4 endometrial areas per section were acquired for analysis with ImageJ software (National Institute of Health, open source software; imagej.nih.gov/ij/). Nuclei were scored numerically by the computer software based on staining intensity on a 0 to 255 scale. Nuclei scoring with ≥30% intensity were considered positive for PR. A minimum of 1000 cells were counted for each animal, and a labeling index (%) for LE and GE was calculated by tabulating the number of positively-labeled cells and dividing it by the total number of cells counted for that section area and cell compartment. Stromal staining was not quantified due to insufficient intensity of signal for quantification by ImageJ; however, PR labeling was present in stromal cells as well (Figure 9, next section).

3.3 Statistical Analysis

Quantitative data (Ki67 and PR LI) were subjective to analyses of variance (ANOVA) using the general linear model procedures available with SAS® software (SAS Institute Inc., SAS 9.1.3, Cary, NC). Statistical models considered variation associated with age (e.g. prenatal and postnatal categories by week), cell compartment (e.g. GE, LE, and ST) and their interaction as appropriate. Error terms used in tests of significance were based upon expectations of the mean square for error for a mixed model where foal (a random source of variation) was nested within age category. Where more than two categories were represented for a component of the model (ex. age), preplanned orthogonal contrasts were performed to evaluate the nature of such potential effects. Results are expressed as least squares means with standard error of the mean.

IV. Results

4.1 Uterine Histology

A summary of observations related to effects of age, from pre- to postnatal periods, on equine uterine histology is presented in Table 7. Representative photomicrographs of uterine sections from each age group category are presented in Figures 1 and 2. All tissue specimens examined contained all primary tissue layers, including endometrium (stratum compactum [SC] and stratum spongiosum [SS]), myometrium (MYO), and perimetrium (PERI). In the fetal age group (GD 300-337; Figure 3A), epithelial budding, indicative of the emergence of nascent endometrial glands, was noted at the apex of endometrial folds. Evidence of tubulogenesis and coiling of nascent GE was also noted, predominantly at the base of endometrial folds, which were longitudinal ridges of glandless connective tissue covered by endometrium on both sides as described by Kenney in 1978 (3). Uteri obtained from early postnatal animals (PND 0-6; Figure 3B) exhibited a similar phenotype, with more extensive gland development at the base of endometrial folds, and sporadic development of glands at the apex of endometrial folds. Mid-postnatal animals (PND 23-32; Figure 3C) displayed a more varied phenotype, with two animals (both PND 23) having more prominent glandular development compared to the other uteri examined in this age group. Foals in this age group had endometrial glands at the apex of endometrial folds, with tubulogenesis, coiling and branching evident in groups of glands at the base of endometrial folds. Occasional areas with extensive branching and coiling were noted, but

gland penetration depth was limited to the stratum compactum. Uteri from late postnatal foals (PND 45-180; Figure 3D) displayed more advanced branching and coiling, which was especially prominent at the base of the endometrial folds and, in some cases, extended to the apex of these folds as well. Gland penetration depth did not extend beyond the stratum compactum, even in the oldest animals examined (PND 180; Figure 4).

Table 7: Histologic Descriptions

Foal Age	Number of Animals	Tissue layers present	Endometrial Glands	Remarks
Fetal: *GD 300 (3), GD 320 (2), GD 337 (1),*	6	SC, SS, MYO, PERI	Primitive gland structures with some branching, exclusively at the base of the endometrial folds. Budding glands at the apex of the folds.	Glands contained within the SC
Early Postnatal: *PND 0 (5), PND 1 (1), PND 2 (1), PND 6 (1)*	8	SC, SS, MYO, PERI	Tubulogenesis present at the base of the endometrial folds and focally along the apex of the endometrial folds. Some branching noted at base of folds	Glands contained within the SC
Mid Postnatal: *PND 23 (2), PND 25 (1), PND 26 (1), PND 27 (3), PND 28 (3), PND 29 (1), PND 30 (1), PND 32 (1)*	13	SC, SS, MYO, PERI	Tubulogenesis consistently at the apex of the endometrial folds with branching and coiling at the base of the endometrial folds; focal areas at base of folds with extensive branching consistent with adult phenotype but lacking depth beyond SC	Animals #9,#14 (PND 23) had more extensive gland structures than expected for age when compared to cohort.
Late Postnatal: *PND 45 (1), PND 49 (1), PND 50 (1), PND 70 (1), PND 180 (2)*	6	SC, SS, MYO, PERI	More extensive budding and tubulogenesis at the apex of endometrial folds, and more extensive branching/coiling at base of endometrial folds.	Glands do not penetrate beyond SC, even in PND 180 specimens.

Table of histologic descriptions by age group. Abbreviations: gestational day (GD); postnatal day (PND); stratum compactum (SC); stratum spongiosum (SS); myometrium (MYO); perimetrium (PERI).

Figure 3: Representative Histology Sections

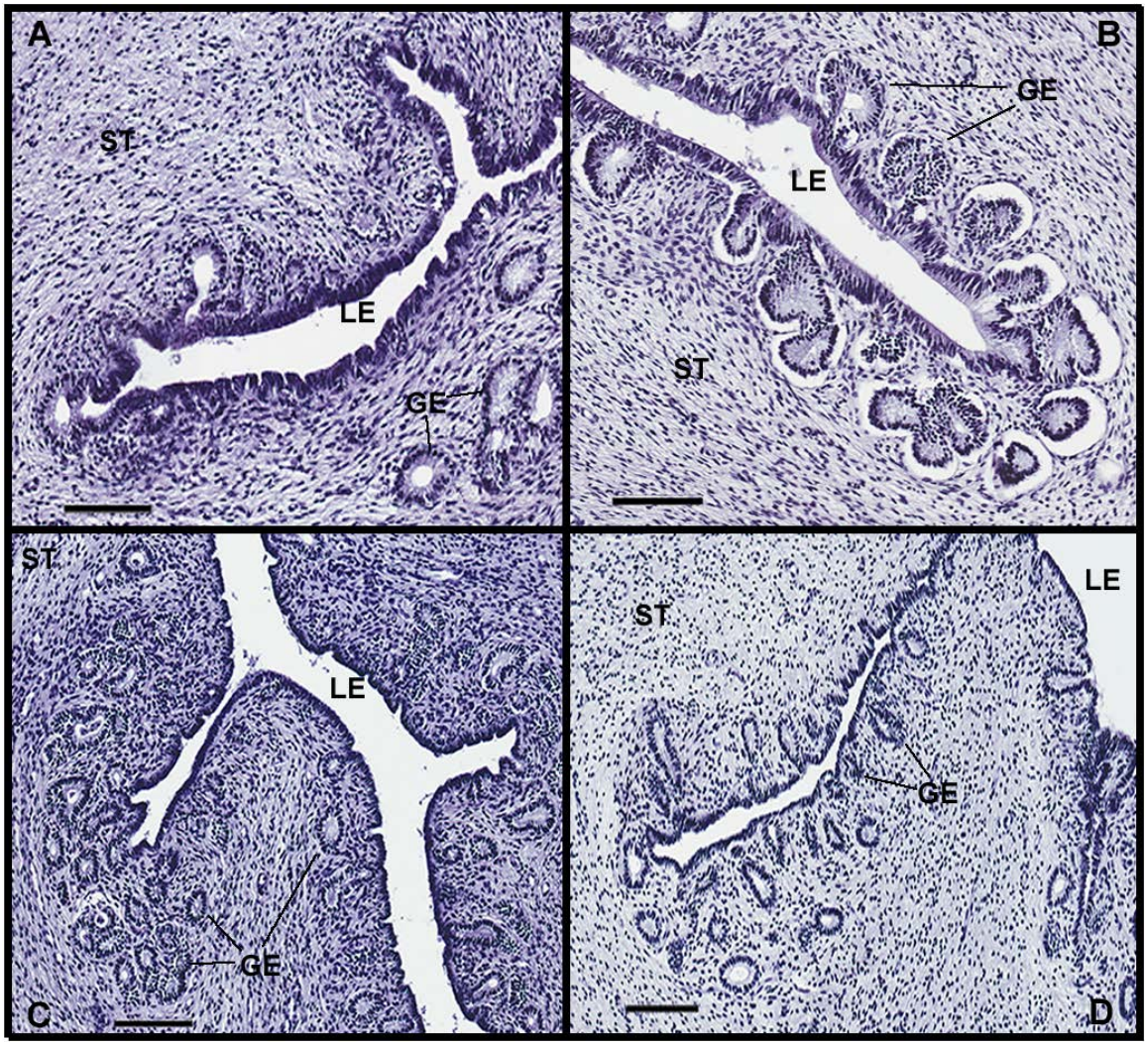

Representative photomicrographs (original magnification 20x) depicting hematoxylin- stained endometrial sections from fetal (A- GD 300), early postnatal (B- PND 6), mid postnatal (C- PND 28), and late postnatal (D- PND 49) equine uteri. LE= luminal epithelium; GE= glandular epithelium; ST= stroma. Scale bar= 100 um.

Figure 4: Histology Section, PND 180

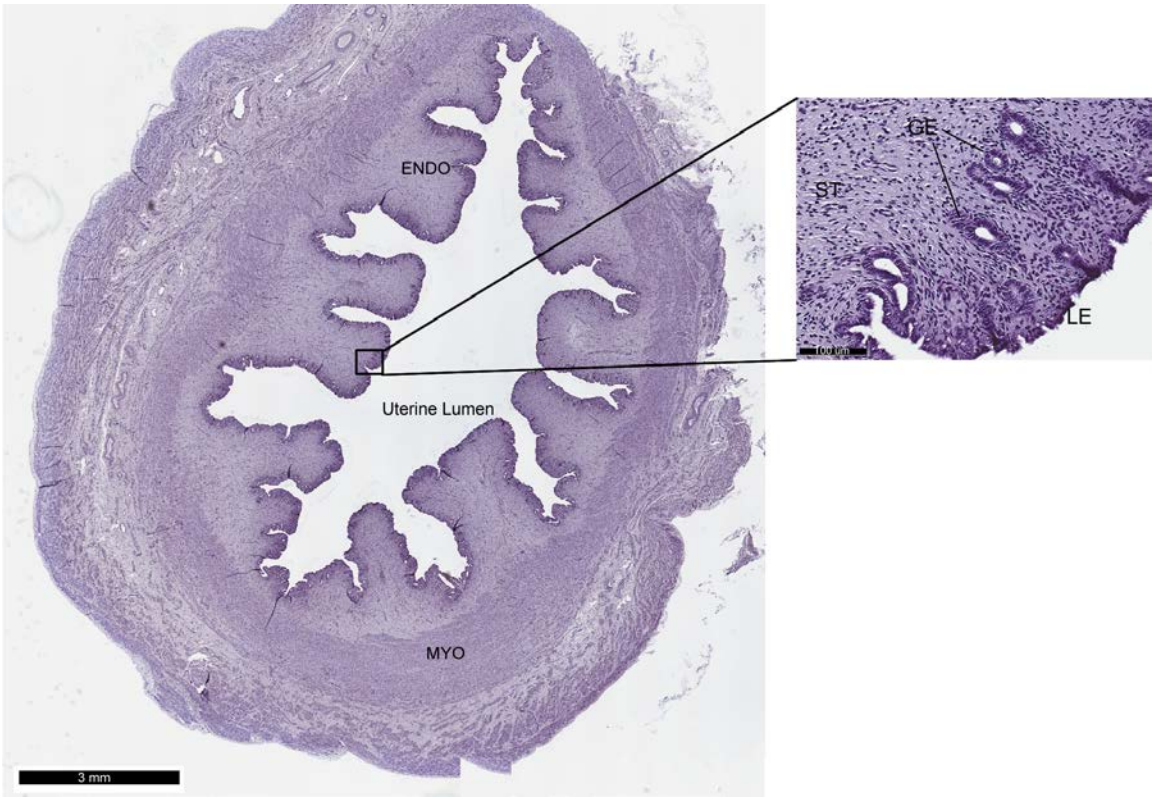

The image above depicts a typical uterine cross section from a PND 180 foal. Endometrial glands do not extend through the stratum compactum and stratum spongiosum as described for the adult phenotype. Endometrium (ENDO), myometrium (MYO), stroma (ST), glandular epithelium (GE), and luminal epithelium (LE) are labeled for reference. Scale bar= 3mm in main image. Scale bar = 100 um in inset.

4.2 Ki67 Labeling Index

Results of a typical Ki67 MSI experiment are presented in Figure 5. Representative, spectrally unmixed composite images generated using MSI for uterine endometrium stained for Ki67 (pink), CK8 (yellow) and DNA (cell nuclei; blue) are presented in Figure 5. Images depict representative endometrial staining patterns for tissues obtained during fetal (GD 300, Figure 5A) and postnatal [weeks 1(PND 0, Figure 5B), 5 (PND 26 and 29, Figure 5C, D), 7 (PND 45, Figure 5E), and 24 (PND 180, 5F] periods. Complementary, spectrally unmixed images depicting Ki67-specific signal alone (A594) are presented in Figure 6A-F. Ki67 positive cells were identified in GE, LE, and ST at all age groups. Positive cells were randomly scattered throughout all three cell compartments and did not demonstrate a uniform pattern of distribution at any age group.

Endometrial cell proliferation index (%), determined by the distribution of Ki67-positive cells, was calculated for: stroma (deep and superficial), and epithelium (GE and LE) for each age group category. Labeling index data are reported as LSM±SE. Data for Ki67 LI (%) are summarized in Figure 7. Results are shown by age category (pre- and postnatal) for epithelium (LE and GE) and stroma (ST). Overall, main effects of age ($P = 0.005$), cell compartment (GE, LE, ST; $P < 0.0001$) and an age by cell compartment interaction ($P < 0.0001$) were identified. Consistent with observations based on results of IHC studies, Ki67 LI increased ($P < 0.0001$) from the prenatal to the postnatal period, and was higher overall ($P < 0.0001$) in epithelium (GE and LE) versus ST. Postnatally, Ki67 LI increased ($P < 0.0001$) from week 1 to week 24.

Figure 5: Representative images, Ki67 Labeling

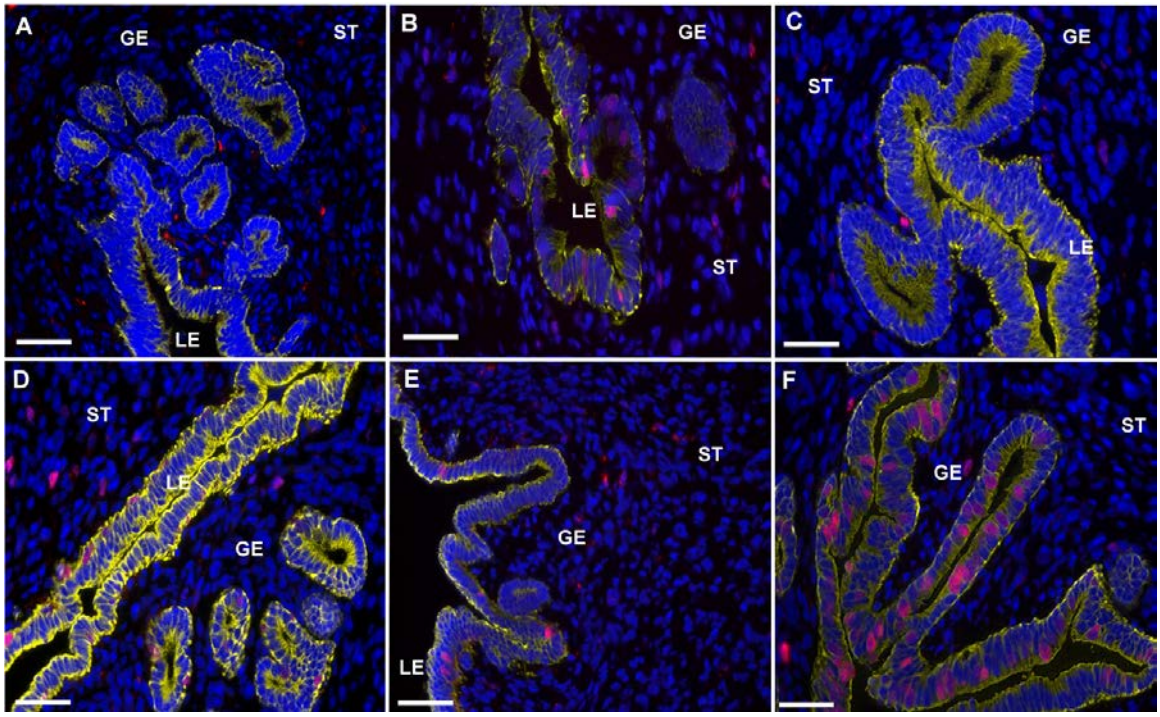

An example series of Ki67- labeled equine endometrium across multiple age groups. Individual animals were grouped by age for statistical analysis; Fetal (A- GD 300), Week 1 (B- PND 0), Week 5 (C- PND 26; D- PND 29), Week 7 (E- PND 45), and Week 24 (F- PND 180). Scale bar= 50 um.

Figure 6: Representative Images, Ki67 Labeling, AF594

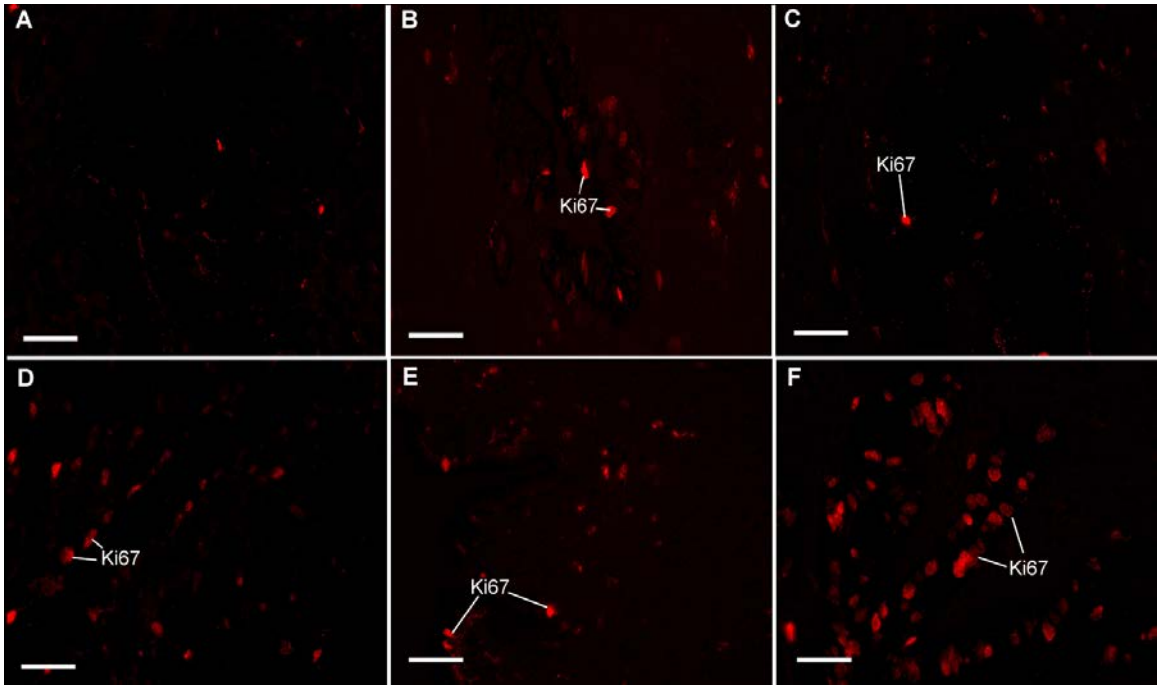

Images 5A-F are the same images depicted in 4A-F, but have been spectrally unmixed to allow viewing of the AF594 channel depicting nuclear staining for Ki67. Positively labeled nuclei are stained red. Fetal (A- GD 300), Week 1 (B- PND 0), Week 5 (C- PND 26; D- PND 29), Week 7 (E- PND 45), and Week 24 (F- PND 180). Scale bar= 50 um.

Figure 7: Ki67 Labeling Index in Glandular Epithelium, Luminal Epithelium, and Stroma

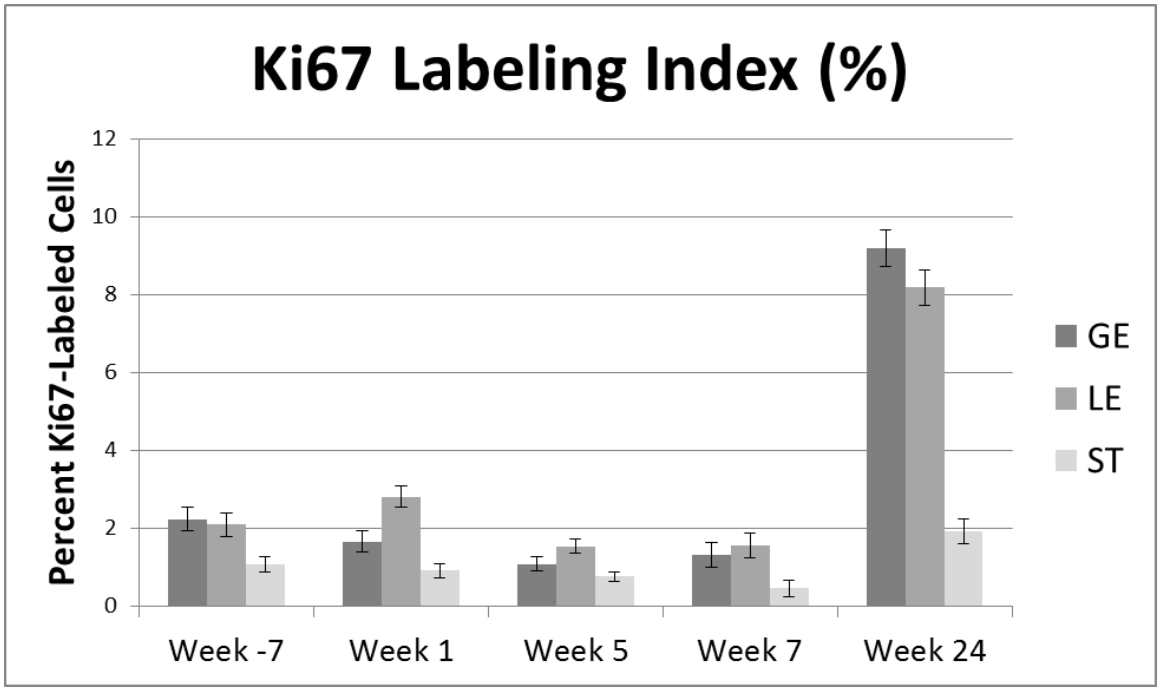

Figure 7 shows the differences in Ki67 labeling index between equine endometrial epithelium and stroma. Data was reported as LSM±SE. Overall, main effects of age ($P = 0.005$), cell compartment (GE, LE, ST; $P < 0.0001$) and an age by cell compartment interaction ($P < 0.0001$) were identified. Consistent with observations based on results of IHC studies, Ki67 LI increased ($P < 0.0001$) from the prenatal to the postnatal period, and was higher overall ($P < 0.0001$) in epithelium (GE and LE) versus ST. Postnatally, Ki67 LI increased ($P < 0.0001$) from week 1 to week 24.

4.3 Endometrial PR Immunostaining

Representative images illustrating patterns of nuclear PR immunostaining for equine endometrial tissues obtained during prenatal (GD 300) and postnatal (PND 6 and PND 29) are presented in Figure 8 (A-C). Overall, results indicated that PR-positive cells are found in both stromal and epithelial compartments throughout the period studied. Regardless of age category, immunostaining intensity for PR was consistently most pronounced in GE (Figure 8). While nuclear staining for PR was evident in stroma, PR LI was not determined for endometrial stroma owing to technical difficulty associated with assessing labeling intensity as necessary to define a signal for PR at or above a threshold value (Figure 9). Consequently, efforts to determine PR LI focused on epithelium.

Data for PR LI (%) are summarized in Figure 10 and are expressed as a percentage of positively labeled cells across three postnatal age groups for which adequate numbers of uterine samples of sufficient quality to permit immunolocalization and visualization of PR were available. Results are shown by age category (pre- and postnatal) for luminal epithelium and glandular epithelium and reported as LSM±SE. Overall, a main effect of cell compartment (GE, LE; $P < 0.0001$) and an age by cell compartment interaction ($P = 0.01$) were identified. Consistent with observations based on results of IHC studies, PR LI was higher in GE than LE for all age groups.

Figure 8: Representative Images, Progesterone Receptor Staining

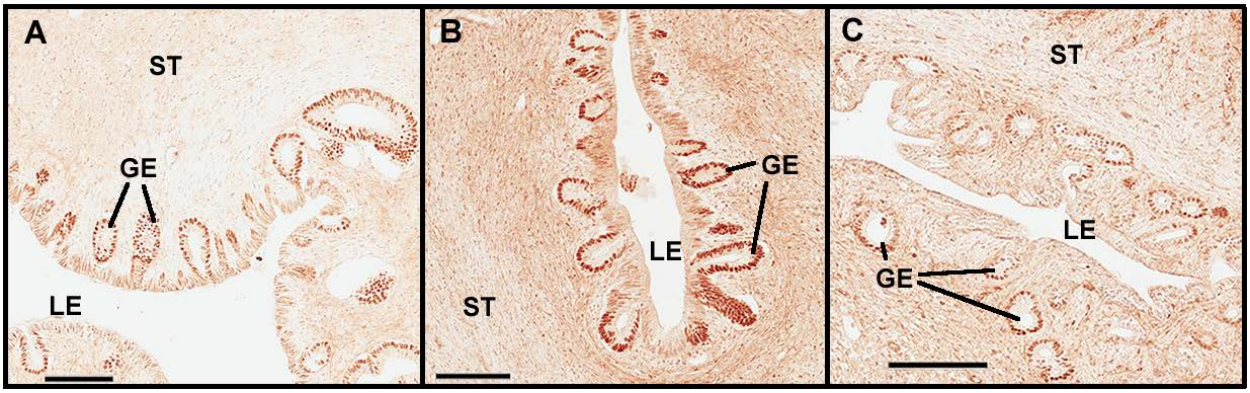

Photomicrographs in figure 8 are representative of PR staining in equine fetal and neonatal endometrium with DAB as the chromogenic reporter. A labeling index was calculated for GE and LE. Nuclei in the stroma demonstrated positive staining for PR, but were not quantified. Animal ages include GD 300 (A), PND 6(B), and PND29 (C). Scale bar= 100um; abbreviations: glandular epithelium (GE); luminal epithelium (LE), and stroma (ST).

Figure 9: PR Immunostaining, PND 50

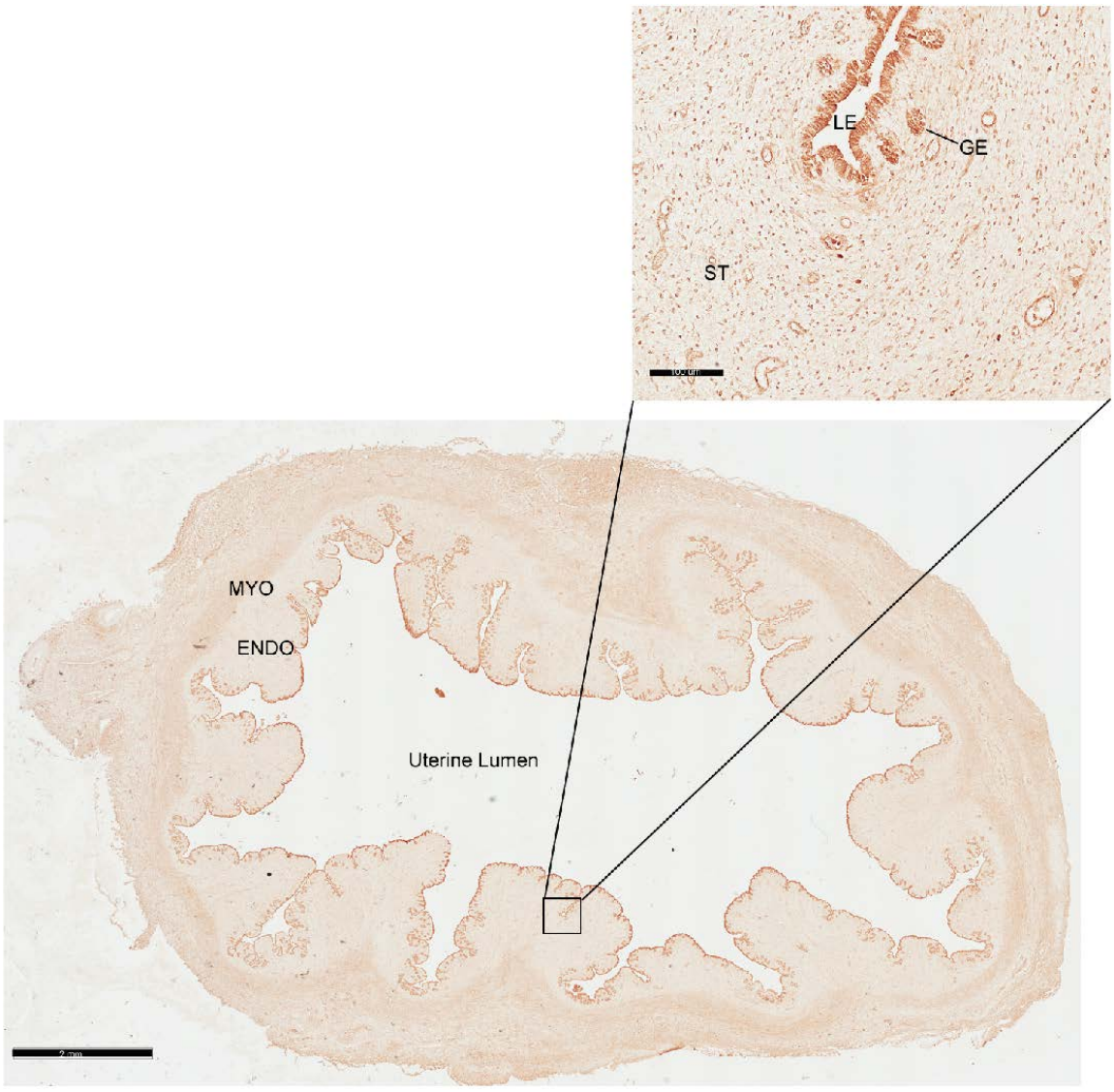

Photomicrographs in figure 9 are representative of PR staining in equine neonatal endometrium (PND 50) with DAB as the chromogenic reporter. Positively-labeled cells for PR are evident in GE, LE, and stroma (inset). Original image procured at 20X magnification; scale bars= 3mm (main image) and 100 μm (inset). Abbreviations: myometrium (MYO), endometrium (ENDO), luminal epithelium (LE), glandular epithelium (GE), stroma (ST).

Figure 10: PR Labeling Index in Equine Endometrium, Glandular vs. Luminal Epithelium

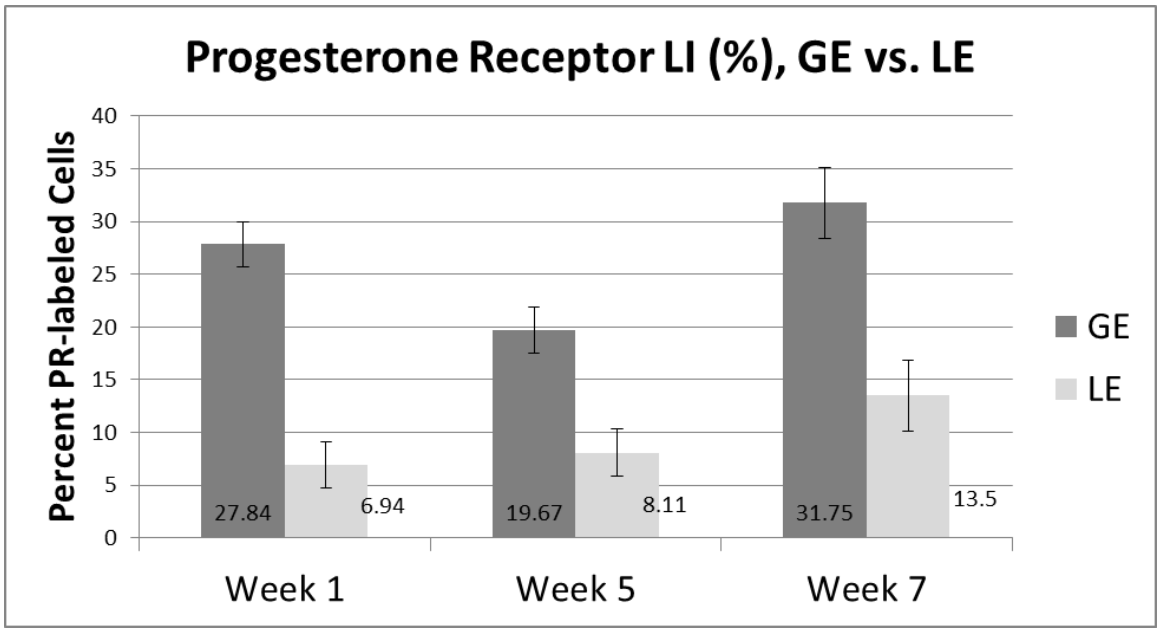

Figure 10 depicts PR labeling index in the glandular and luminal epithelial cell compartments of equine endometrium. Data was expressed as LSM±SE. PR expression was higher in GE compared to LE for each age group ($p<0.001$ for each age category). A significant age by cell compartment interaction was noted ($p=0.01$).

V. Discussion

5.1 Study limitations

There are several study limitations that may impact the interpretation of results. Although an acceptable total number of tissue samples were available for this project, the relative distribution of foals across various age categories was suboptimal and may have prevented potential critical developmental windows from being identified; most notably, the overall lack of foals between PND 6 and PND 23 resulted in a large gap in the age ranges examined. Because of such limitations, foals were grouped together in relative age ranges by pre- or postnatal stage and/or week. In other species such as the mouse (74), time spans as short as a single day can have profound effects on cell behaviors associated with endometrial development. In this light, it is reasonable to assume that some of these changes may have been missed in the present study, particularly in the first week of life. Other factors including artifacts due to tissue autolysis and handling based on the methods of collection must also be considered. Although it may have been more ideal to use purpose-bred animals for this project, where absolute control over tissue collection and processing protocols could be exercised, the cost of such studies involving horses are prohibitive and extremely time consuming based on the gestation length of the mare (340 days).

Availability of antibodies compatible for use in large animals (particularly the horse) is another critical limitation of this kind of research. Very few primary antibodies

are validated for such purposes.

5.2 Conclusions

Histogenesis of the equine endometrium in the samples evaluated in this study was consistent with previous observations by Gerstenberg and Allen (67). This is similar to domestic ungulates where radial patterning and distinct tissue layers of endometrium, myometrium, and stroma are present at birth but differs from mice where the uterus is comprised of poorly differentiated mesenchyme at birth. Humans also exhibit radially patterned stroma at birth with defined zones of endometrium and myometrium, similar to the horse. Endometrial glands were present in all of the fetal tissue samples examined. This is consistent with previous reports that equine uterine gland development is initiated at approximately gestational day 200-250. This is different from other domestic species studied, such as the mouse, ewe (195), sow, cow (196) and bitch (73) where gland genesis occurs nearly exclusively postnatally. Therefore the equine uterus is at a relatively advanced developmental state relative to other domestic species; this degree of development is more similar to humans than domestic animals, where gland genesis is also initiated prenatally. Thus, completion of equine uterine development occurs over a much more prolonged period of time relative to other domestic species; at 24 weeks of age glands were present but penetration depth was still shallow. This is again most similar to humans where uterine adenogenesis occurs over a period of years, with uterine glands penetrating one-half to one-third of the endometrium by six years of age, and mature histoarchitecture is not achieved until puberty (197). Other domestic mammals demonstrate rapid endometrial development with histologic maturity occurring at a much

earlier chronological age; in gilts, histological maturity of the uterus occurs even prior to the onset of cyclicity and puberty (69).

Markers of cell proliferation have been assessed in several other species, including BrDU labeling indices in the pig (78), and Ki67 labeling indices in the mouse (74), and dog (73). In these species, cell proliferation is elevated either at birth or shortly thereafter and does vary by cell compartment but is generally higher in epithelium than stroma (73, 74, 78). This is in contrast to equine endometrial cell proliferation, which is low during late fetal life and at birth but increased with increasing age. Although it is logical that the initiation of gland development would be accompanied by an increase in cell division in the endometrium, it is impossible to definitively conclude without further study since no tissues from animals younger than GD 300 were available for the present study. Cell proliferation indices in neonatal human uterus are unknown at this time. In addition to overall cell proliferation rate, temperospatial patterning of cell proliferation differs in the foal uterus compared to pigs (78). In foals, Ki67 labeled cells appeared scattered at random throughout LE, GE, and ST at all age groups in this study, with no difference in labeling index between GE and LE. This is in contrast to neonatal pigs (PND 14) (78), dogs (2-8 weeks of age) (73) where labeling index is higher in GE compared to LE, with areas of BrDU or Ki67 staining clearly visible in budding endometrial glands. This also differs from mice, where cell proliferation index is high in mice early in the postnatal period (PND10) in both EPI and ST. Species differences may indicate that finite local control over endometrial adenogenesis is less important in equids compared to other domestic species.

Previous studies in adult mares (14, 15) have demonstrated the presence of PR in both luminal and glandular epithelium at approximately the same rate of staining intensity in glandular and luminal epithelium; however, staining intensity was described by the authors as “moderate”, rather than being expressed as a percentage of total cells. Thus, it is difficult to make a direct comparison between the distribution of PR in foal and adult mare endometrium. The presence of PR in both glandular and luminal epithelium at all age groups implies that there is the potential for action of progestins on the foal uterus, and the anti-proliferative effects of progestins (198-200) and glucocorticoids (201) are previously documented. Gland genesis in equids is initiated during a time period where the fetus is exposed to high levels of progestins, thus progesterone and similar compounds likely do not have an inhibitory effect on uterine gland development in late fetal life. This does not mean, however, that endometrial adenogenesis in equids is not steroid sensitive. In pigs, disruption of endometrial adenogenesis was achieved by administering ICI 182,780, which is a type-II ER antagonist; it is possible that equine endometrial adenogenesis could be altered through a similar mechanism by blocking estrogen signaling. Early endometrial adenogenesis in other species studied to date is ovary-independent. This has not been conclusively determined in equids. Nakai and colleagues (202) assessed levels of LH, FSH, inhibin, P4, E2, and testosterone in fillies from birth to 6 months of age, and showed that plasma levels of sex steroid hormones decreased rapidly within 48 hours of birth and remained low until 6 months of age. Therefore, it is unlikely that the ovary is producing endocrine compounds that impact endometrial development in equids.

Taken together, histologic descriptions and labeling index data imply that the equine endometrium is at a relatively inactive developmental state between late gestation and up to 24 weeks of age, with an increase in proliferation in all cell compartments beginning at approximately 24 weeks of age. This is markedly different from other species studied to date. This may in part explain the failure to generate a UGKO-phenotype when treating foals with altrenogest and estrogen during this time period, as the endometrium may not be sensitive to these compounds during this time frame, or at all, during perinatal life (66). As the rate of cell division increased in the oldest age group, disruption of normal adenogenesis may be possible with administration of steroid hormones during a later period of time.

Of equal importance, this study demonstrates application for the use of multi-spectral imaging in equine tissue. A major limiting step in advancement with this analytical technique is the availability of primary antibodies applicable for use in equine tissues. Further assessment of tissue handling techniques is needed to determine optimal fixation protocols for use in equine tissue that maximizes both antigen identification and preservation of tissue architecture. Manual counting of cells was necessary in this study to overcome limitations associated with the CellProfiler™ and CellProfiler Analyst™ software, but this introduces bias based on the number of individuals counting as well as inherent variability in what level of staining is present before the operator classifies the cell as positively labeled.

5.3 Acknowledgements

Authors declare there is no conflict of interest that could be perceived as prejudicing the impartiality of the research. Authors acknowledge collaborators at The

University of Kentucky College of Agriculture, Food, and Environment, Gluck Equine Research Center Department of Veterinary Science and Veterinary Diagnostic Laboratory, notably Dr. I. Canisso for obtaining tissue samples and Dr. L. Kennedy for assistance with acquiring additional tissues. This work was supported by the Birmingham Racing Commission (to Wilborn). Work involving vertebrate animals was approved by the University of Kentucky Institutional Animal Care and Use Committee.

Appendix A: Immunofluorescent Staining Protocol

Materials:

1. Desired primary antibodies (table 1)
2. Desired secondary antibodies (table 2)
3. Acetone, chilled to -20° C
4. PAP/immunopen
5. VectaShield Mounting Medium for Fluorescence with DAPI: Vector Laboratories
6. Non-immune Goat Serum: Vector Laboratories
7. 1X PBS
8. Warm air dryer (hair dryer)

Procedure for immunofluorescent labeling: (as adapted from M. Davolt, 2015)

1. Section tissues at 6 um thick using cryostat
2. Mount 2 non-sequential sections on VWR Superfrost®Plus glass slides.
3. Allow slides to dry for 2-3 minutes, then transfer to cold slide box in -20C° freezer.
4. To fix sections:
    a. Remove desired slides from freezer; dry with warm air (low heat setting) for 60 seconds
    b. Submerge slides in chilled acetone for 5 minutes
    c. Remove slides from acetone, and allow to dry at room temperature for 10 minutes to evaporate acetone
5. Wash in 1X PBS 2 times for 3 minutes each.

6. Prepare 2 containers of 1X PBS.
7. Circle individual sections with immuopen.
8. Block with 10% non-immune goat serum for 60 minutes at room temperature
9. Apply primary antibody cocktail; allow to incubate for 60 minutes at room temperature
10. Wash slides in 1X PBS 2 times for 3 minutes each.

*****The remaining steps should be performed in dim light*****

11. Centrifuge secondary antibody stock solutions to remove particulate matter and dilute as listed;
12. Apply secondary antibody cocktail.
13. Incubate in dark, humidified chamber for 60 minutes at room temperature.
14. Wash in 1X PBS two times, for three minutes each.
15. Apply Vectashield mouting media for fluorescence with DAPI;
    a. DAPI should be allowed to equilibrate for at least 5 minutes prior to imaging
    b. slides can be stored at 4°C in a dark box for imaging within the next 12-24 hours.

Appendix B: Digital Image Analysis: CellProfiler™ Analyses of Fluorescent Signals

Adapted from M. Davolt, 2015

Materials

1. CellProfiler™ Image Analysis software (downloaded www.cellprofiler.com)
2. CellProfiler™ Analyst software (downloaded www.cellprofiler.com)
3. Spectrally unmixed component data files
4. Identified input folder
5. Identified output folder

Quantitative data collection was attmpted using CellProfiler™. wavelength-specific image data sets were uploaded, epithelial (LE+GE) and stromal cell compartments were identified using CK8 mask (direct and inverted, respectively), cell nuclei were identified within each cell compartment, measurements of signal intensity were collected and data sets were exported for data analysis.

Pipeline name: EPI vs. ST

1. Load Images: Loads and extracts metadata from first component image in image set
2. Load Single Image: Loads a single image for use in all image cycles
3. Apply Threshold: Sets pixel intensities below or above a certain threshold to zero producing a binary image for component image corresponding to AlexaFluor 594 (Ki67)
4. Apply Threshold: Repeated for component image corresponding to AlexaFluor 546 (CK8)

5. Apply Threshold: Repeated for component image corresponding to DAPI
6. Image Math: Performs basic mathematical operations on image intensities; Binary images produced from 'Apply Threshold' modules for component images corresponding to AlexaFluor 594, 546, and DAPI were added and renamed 'total'
7. Mask Image: Hides certain portions of an image (based on previously identified objects or a binary image) so they are ignored by subsequent mask-respecting modules in the pipeline; performed on component image corresponding to AlexaFluor 546.
8. Mask Image: Repeated for component image corresponding to AlexaFluor 594
9. Mask Image: Repeated for component image corresponding to DAPI.
10. Identify Primary Objects: Identifies objects in an image; The component image corresponding to AlexaFluor 546 was used to identify the epithelium (targets Cytokeratin 8, unique structural protein of epithelial cells)
11. Expand or Shrink Objects: Expands or shrinks objects by a defined distance
12. Convert Objects to Image: Converts objects you have identified into an image (forms CK8 "mask")
13. Mask Image: Resulting image from 'Convert Objects to Image' was applied as a mask to the component image corresponding to cell nuclei (DAPI) to hide all stromal nuclei (NB: in the stromal pipeline, this was inverted to hide all epithelial cell nuclei)
14. Identify Primary Objects: Identifies epithelial nuclei (NB: due to mask inversion in the stromal pipeline, this identified stromal nuceli)

15. Measure Object Size Shape: Measures several area and shape features of identified objects
16. Measure Texture: Measures the degree and nature of textures within objects (versus smoothness)
17. Measure Object Intensity: Measures several intensity features for identified objects
18. Measure Granularity: Outputs spectra of size measurements of the textures in the image
19. Overlay Outlines: Places outlines produced by an Identify module over a desired image
20. Save Images: Saves images or movie files
21. Export to Database: Exports data directly to a database, or in database readable format, including an imported file with column names and a CellProfilerTM Analyst properties file; Select “single object table”
22. Export to Spreadsheet: Exports measurements into one or more files that can be opened in Excel or other spreadsheet programs; This is especially helpful when metadata is used
23. View Output Settings: select the desired output folder for data; this will automatically become part of the properties file for CPA

Digital Image Analysis: CellProfiler™ Analyst

CellProfiler™ Analyst exported measurement files and thumbnail images from CellProfiler™ were used to identify cell behavior and phenotype.

Creating CellProfiler™ Analyst rule definitions:

1. Open CellProfilerTM Analyst from your desktop, when prompted open the ‘EPI’ or ‘ST” properties file saved from previous CellProfilerTM run.
2. Select the Classifier icon on the tool bar
3. Edit color assignment of wavelength-specific channels from the drop down menu to match expected color (ie, change Ki67 to red, DAPI to blue, etc)
4. Select View from tool bar to adjust size of thumbnails (maximize)
5. Assign bins located at the bottom of the window: Ki67 positive, Ki67 negative
6. Select the number of thumbnails to view in the window next to ‘Fetch’ (100 is suggested) ; select ‘random’ from the drop down menu
7. Click ‘Fetch!’
8. 100 thumbnails from your experiment will appear in the ‘unclassified cells’ window
9. Click and drag thumbnails to desired bins- the dot in each image is on the nuclei the algorithm will classify
10. Once you’ve identified some cells in each category click ‘Train Classifier’
    a. This will build an algorithm based on your selections
    b. The ‘rules’ or definitions created by manual cell sorting will appear in the window above the thumnails
    c. Aim- exclude any ‘rules’ that include size, shape, location etc. (the focus of the algorithm must be on signal intensity measurements only to allow downstream application in CellProfiler™)
11. Once you’ve identified 10-15 cells in each category test your algorithm by selecting ‘Check Progress’

a. A window displaying a line graph named ‘cross validation accuracy’ will appear
b. As per the CellProfiler™ manual: a cross validation accuracy of 80% or more should be aimed for if 2 bins are used, if 3 or more bins are used a cross validation accuracy of 90% or more should be aimed for.

12. Return to the Classifier window and save your workspace by File>Save Workspace
13. For this experiment the following bin pairs was made: Ki67-positive, Ki67-negative
14. Select and copy ‘rules’ for the positive-negative pair in plain text format

Cross-validation accuracy did not meet necessary thresholds; CP/CPA image analysis was abandoned at that time.

Appendix C: EPI Properties File

```
#Thu Nov  5 13:13:51 2015
# ================================================
#
# CellProfiler Analyst 2.0 properties file
#
# ================================================
# ==== Database Info ====
db_type         = sqlite
db_sqlite_file  = D:\Fraser MS\EPI.db
# ==== Database Tables ====
image_table   = Per_Image
object_table  = Per_Object
# ==== Database Columns ====
# Specify the database column names that contain unique IDs for images and
# objects (and optionally tables).
#
# table_id (OPTIONAL): This field lets Classifier handle multiple tables if
#          you merge them into one and add a table_number column as a foreign
#          key to your per-image and per-object tables.
# image_id: must be a foreign key column between your per-image and per-object
#          tables
# object_id: the object key column from your per-object table
```

image_id = ImageNumber

object_id = ObjectNumber

plate_id =

well_id =

Also specify the column names that contain X and Y coordinates for each

object within an image.

cell_x_loc = EPInuclei_Location_Center_X

cell_y_loc = EPInuclei_Location_Center_Y

==== Image Path and File Name Columns ====

Classifier needs to know where to find the images from your experiment.

Specify the column names from your per-image table that contain the image

paths and file names here.

#

Individual image files are expected to be monochromatic and represent a single

channel. However, any number of images may be combined by adding a new channel

path and filename column to the per-image table of your database and then

adding those column names here.

#

NOTE: These lists must have equal length!

image_path_cols =

Image_PathName_CK8546,Image_PathName_DAPI,Image_PathName_KI67594,Image

_PathName_overlayEPI

image_file_cols =

Image_FileName_CK8546,Image_FileName_DAPI,Image_FileName_KI67594,Image_FileName_overlayEPI

CPA will now read image thumbnails directly from the database, if chosen in ExportToDatabase.

image_thumbnail_cols =

Image_Thumbnail_CK8546,Image_Thumbnail_DAPI,Image_Thumbnail_KI67594,Image_Thumbnail_overlayEPI,Image_Thumbnail_CK8546noaf,Image_Thumbnail_CK8mask,Image_Thumbnail_DAPIepi,Image_Thumbnail_DAPInoaf,Image_Thumbnail_ImageAfterMath,Image_Thumbnail_KI67594noaf,Image_Thumbnail_ThreshCK8,Image_Thumbnail_ThreshDAPI,Image_Thumbnail_ThreshKI67

Give short names for each of the channels (respectively)...

image_names = CK8546,DAPI,KI67594,overlayEPI

Specify a default color for each of the channels (respectively)

Valid colors are: [red, green, blue, magenta, cyan, yellow, gray, none]

image_channel_colors = red, green, blue, cyan, magenta, yellow, gray, none, none, none, none, none, none

==== Image Accesss Info ====

image_url_prepend =

==== Dynamic Groups ====

Here you can define groupings to choose from when classifier scores your experiment. (eg: per-well)

This is OPTIONAL, you may leave "groups = ".

FORMAT:

group_XXX = MySQL select statement that returns image-keys and group-keys. This will be associated with the group name "XXX" from above.

EXAMPLE GROUPS:

groups = Well, Gene, Well+Gene,

group_SQL_Well = SELECT Per_Image_Table.TableNumber, Per_Image_Table.ImageNumber, Per_Image_Table.well FROM Per_Image_Table

group_SQL_Gene = SELECT Per_Image_Table.TableNumber, Per_Image_Table.ImageNumber, Well_ID_Table.gene FROM Per_Image_Table, Well_ID_Table WHERE Per_Image_Table.well=Well_ID_Table.well

group_SQL_Well+Gene = SELECT Per_Image_Table.TableNumber, Per_Image_Table.ImageNumber, Well_ID_Table.well, Well_ID_Table.gene FROM Per_Image_Table, Well_ID_Table WHERE Per_Image_Table.well=Well_ID_Table.well

==== Image Filters ====

Here you can define image filters to let you select objects from a subset of your experiment when training the classifier.

FORMAT:

filter_SQL_XXX = MySQL select statement that returns image keys you wish to filter out. This will be associated with the filter name "XXX" from above.

EXAMPLE FILTERS:

filters = EMPTY, CDKs,

filter_SQL_EMPTY = SELECT TableNumber, ImageNumber FROM CPA_per_image, Well_ID_Table WHERE CPA_per_image.well=Well_ID_Table.well AND Well_ID_Table.Gene="EMPTY"

filter_SQL_CDKs = SELECT TableNumber, ImageNumber FROM CPA_per_image, Well_ID_Table WHERE CPA_per_image.well=Well_ID_Table.well AND Well_ID_Table.Gene REGEXP 'CDK.*'

==== Meta data ====

What are your objects called?

FORMAT:

object_name = singular object name, plural object name,

object_name = cell, cells,

What size plates were used? 96, 384 or 5600? This is for use in the PlateViewer. Leave blank if none

plate_type =

==== Excluded Columns ====

OPTIONAL

Classifier uses columns in your per_object table to find rules. It will

automatically ignore ID columns defined in table_id, image_id, and object_id

as well as any columns that contain non-numeric data.

#

Here you may list other columns in your per_object table that you wish the

classifier to ignore when finding rules.

#

You may also use regular expressions here to match more general column names.

#

Example: classifier_ignore_columns = WellID, Meta_.*, .*_Position

This will ignore any column named "WellID", any columns that start with

"Meta_", and any columns that end in "_Position".

#

A more restrictive example:

classifier_ignore_columns = ImageNumber, ObjectNumber, .*Parent.*, .*Children.*,

.*_Location_Center_.*,.*_Metadata_.*

classifier_ignore_columns = table_number_key_column, image_number_key_column,

object_number_key_column

==== Other ====

Specify the approximate diameter of your objects in pixels here.

image_tile_size   = 50

======== Auto Load Training Set ========

OPTIONAL

You may enter the full path to a training set that you would like Classifier

to automatically load when started.

training_set =

======== Area Based Scoring ========

OPTIONAL

You may specify a column in your per-object table which will be summed and

reported in place of object-counts when scoring. The typical use for this

```
# is to report the areas of objects on a per-image or per-group basis.

area_scoring_column =

# ======== Output Per-Object Classes ========

# OPTIONAL

# Here you can specify a MySQL table in your Database where you would like

# Classifier to write out class information for each object in the

# object_table

class_table  = cellcalls

# ======== Check Tables ========

# OPTIONAL

# [yes/no]  You can ask classifier to check your tables for anomalies such

# as orphaned objects or missing column indices.  Default is on.

# This check is run when Classifier starts and may take up to a minute if

# your object_table is extremely large.

check_tables = yes
```

Appendix D: ST Properties File

```
#Mon Oct 26 22:16:14 2015
# ============================================
#
# CellProfiler Analyst 2.0 properties file
#
# ============================================
# ==== Database Info ====
db_type         = sqlite
db_sqlite_file  = D:\Fraser MS\ST.db
# ==== Database Tables ====
image_table   = Per_Image
object_table  = Per_Object
# ==== Database Columns ====
# Specify the database column names that contain unique IDs for images and
# objects (and optionally tables).
#
# table_id (OPTIONAL): This field lets Classifier handle multiple tables if
#          you merge them into one and add a table_number column as a foreign
#          key to your per-image and per-object tables.
# image_id: must be a foreign key column between your per-image and per-object
#          tables
# object_id: the object key column from your per-object table
```

image_id = ImageNumber

object_id = ObjectNumber

plate_id =

well_id =

Also specify the column names that contain X and Y coordinates for each

object within an image.

cell_x_loc = STnuclei_Location_Center_X

cell_y_loc = STnuclei_Location_Center_Y

==== Image Path and File Name Columns ====

Classifier needs to know where to find the images from your experiment.

Specify the column names from your per-image table that contain the image

paths and file names here.

#

Individual image files are expected to be monochromatic and represent a single

channel. However, any number of images may be combined by adding a new channel

path and filename column to the per-image table of your database and then

adding those column names here.

#

NOTE: These lists must have equal length!

image_path_cols =

Image_PathName_CK8546,Image_PathName_DAPI,Image_PathName_KI67594,Image

_PathName_overlayST

image_file_cols =

Image_FileName_CK8546,Image_FileName_DAPI,Image_FileName_KI67594,Image_FileName_overlayST

CPA will now read image thumbnails directly from the database, if chosen in ExportToDatabase.

image_thumbnail_cols =

Image_Thumbnail_CK8546,Image_Thumbnail_DAPI,Image_Thumbnail_KI67594,Image_Thumbnail_overlayST,Image_Thumbnail_CK8546noaf,Image_Thumbnail_CK8mask,Image_Thumbnail_DAPInoaf,Image_Thumbnail_DAPIst,Image_Thumbnail_ImageAfterMath,Image_Thumbnail_KI67594noaf,Image_Thumbnail_ThreshCK8,Image_Thumbnail_ThreshDAPI,Image_Thumbnail_ThreshKI67

Give short names for each of the channels (respectively)...

image_names = CK8546,DAPI,KI67594,overlayST

Specify a default color for each of the channels (respectively)

Valid colors are: [red, green, blue, magenta, cyan, yellow, gray, none]

image_channel_colors = red, green, blue, cyan, magenta, yellow, gray, none, none, none, none, none, none

==== Image Accesss Info ====

image_url_prepend =

==== Dynamic Groups ====

Here you can define groupings to choose from when classifier scores your experiment. (eg: per-well)

This is OPTIONAL, you may leave "groups = ".

FORMAT:

group_XXX = MySQL select statement that returns image-keys and group-keys. This will be associated with the group name "XXX" from above.

EXAMPLE GROUPS:

groups = Well, Gene, Well+Gene,

group_SQL_Well = SELECT Per_Image_Table.TableNumber, Per_Image_Table.ImageNumber, Per_Image_Table.well FROM Per_Image_Table

group_SQL_Gene = SELECT Per_Image_Table.TableNumber, Per_Image_Table.ImageNumber, Well_ID_Table.gene FROM Per_Image_Table, Well_ID_Table WHERE Per_Image_Table.well=Well_ID_Table.well

group_SQL_Well+Gene = SELECT Per_Image_Table.TableNumber, Per_Image_Table.ImageNumber, Well_ID_Table.well, Well_ID_Table.gene FROM Per_Image_Table, Well_ID_Table WHERE Per_Image_Table.well=Well_ID_Table.well

==== Image Filters ====

Here you can define image filters to let you select objects from a subset of your experiment when training the classifier.

FORMAT:

filter_SQL_XXX = MySQL select statement that returns image keys you wish to filter out. This will be associated with the filter name "XXX" from above.

EXAMPLE FILTERS:

filters = EMPTY, CDKs,

filter_SQL_EMPTY = SELECT TableNumber, ImageNumber FROM CPA_per_image, Well_ID_Table WHERE CPA_per_image.well=Well_ID_Table.well AND Well_ID_Table.Gene="EMPTY"

filter_SQL_CDKs = SELECT TableNumber, ImageNumber FROM CPA_per_image, Well_ID_Table WHERE CPA_per_image.well=Well_ID_Table.well AND Well_ID_Table.Gene REGEXP 'CDK.*'

==== Meta data ====

What are your objects called?

FORMAT:

object_name = singular object name, plural object name,

object_name = cell, cells,

What size plates were used? 96, 384 or 5600? This is for use in the PlateViewer. Leave blank if none

plate_type =

==== Excluded Columns ====

OPTIONAL

Classifier uses columns in your per_object table to find rules. It will

automatically ignore ID columns defined in table_id, image_id, and object_id

as well as any columns that contain non-numeric data.

#

Here you may list other columns in your per_object table that you wish the

classifier to ignore when finding rules.

#

You may also use regular expressions here to match more general column names.

#

Example: classifier_ignore_columns = WellID, Meta_.*, .*_Position

This will ignore any column named "WellID", any columns that start with

"Meta_", and any columns that end in "_Position".

#

A more restrictive example:

classifier_ignore_columns = ImageNumber, ObjectNumber, .*Parent.*, .*Children.*,

.*_Location_Center_.*,.*_Metadata_.*

classifier_ignore_columns = table_number_key_column, image_number_key_column,

object_number_key_column

==== Other ====

Specify the approximate diameter of your objects in pixels here.

image_tile_size   = 50

======== Auto Load Training Set ========

OPTIONAL

You may enter the full path to a training set that you would like Classifier

to automatically load when started.

training_set =

======== Area Based Scoring ========

OPTIONAL

You may specify a column in your per-object table which will be summed and

reported in place of object-counts when scoring. The typical use for this

```
# is to report the areas of objects on a per-image or per-group basis.

area_scoring_column =

# ======== Output Per-Object Classes ========

# OPTIONAL

# Here you can specify a MySQL table in your Database where you would like

# Classifier to write out class information for each object in the

# object_table

class_table  = cellcalls

# ======== Check Tables ========

# OPTIONAL

# [yes/no]  You can ask classifier to check your tables for anomalies such

# as orphaned objects or missing column indices.  Default is on.

# This check is run when Classifier starts and may take up to a minute if

# your object_table is extremely large.

check_tables = yes
```

Appendix E: EPI pipeline CellProfiler™ Analyst rules

The rules listed below correspond with the cross validational accuracy graphically presented in Figure 2A. 69 postively-labeled cells and 104 negative cells were manually categorized to develop the following rules:

1. IF (EPInuclei_Intensity_MinIntensityEdge_DAPIepi > 0.0208743419498, [-0.80560507471737397, 0.80560507471737397], [0.14117256779591977, -0.14117256779591977])
2. IF (EPInuclei_Granularity_1_DAPIepi > 33.255917623800002, [-0.82548484982166215, 0.82548484982166215], [0.11652677430755776, -0.11652677430755776])
3. IF (EPInuclei_AreaShape_Eccentricity > 0.85900719005600001, [-0.53125611116473204, 0.53125611116473204], [0.13055583362244133, -0.13055583362244133])
4. IF (EPInuclei_AreaShape_Center_X > 366.0, [0.14478412358540027, -0.14478412358540027], [-0.48451471856029799, 0.48451471856029799])
5. IF (EPInuclei_AreaShape_Center_X > 1109.0, [-0.66106277928974877, 0.66106277928974877], [0.10994781130395923, -0.10994781130395923])
6. IF (EPInuclei_Intensity_MinIntensityEdge_DAPIepi > 0.0154421301559, [0.1235704941383453, -0.1235704941383453], [-0.45031335557051966, 0.45031335557051966])
7. IF (EPInuclei_Intensity_IntegratedIntensityEdge_DAPIepi > 8.2195926196899993, [-0.81633333754855653, 0.81633333754855653], [0.078315508744814577, -0.078315508744814577])

8. IF (EPInuclei_Texture_Variance_DAPIepi_3_135 > 2.9197474624900002, [-0.23081587653200658, 0.23081587653200658], [0.2690848700135271, -0.2690848700135271])
9. IF (EPInuclei_Texture_SumEntropy_DAPIepi_3_135 > 2.1481365281499998, [0.082299560995812981, -0.082299560995812981], [-0.84412012379261125, 0.84412012379261125])
10. IF (EPInuclei_Location_MaxIntensity_Y_DAPIepi > 548.0, [-0.38327297348510164, 0.38327297348510164], [0.18620248148780191, -0.18620248148780191])
11. IF (EPInuclei_Granularity_11_DAPIepi > 2.89441080826, [0.28959945114670721, -0.28959945114670721], [-0.26036596630781766, 0.26036596630781766])
12. IF (EPInuclei_Texture_DifferenceVariance_DAPIepi_3_0 > 1.25066884661, [0.65396841611172807, -0.65396841611172807], [-0.10170846281216814, 0.10170846281216814])
13. IF (EPInuclei_AreaShape_Zernike_3_3 > 0.024215930719099998, [-0.30206839915350187, 0.30206839915350187], [0.21496627730519818, -0.21496627730519818])
14. IF (EPInuclei_Intensity_MinIntensityEdge_DAPIepi > 0.0208743419498, [-0.70882686228369285, 0.70882686228369285], [0.1016648787033412, -0.1016648787033412])

15. IF (EPInuclei_Intensity_MassDisplacement_DAPIepi > 0.52878419377200003, [0.16965666638768628, -0.16965666638768628], [-0.31184106576441156, 0.31184106576441156])
16. IF (EPInuclei_Texture_Contrast_DAPIepi_3_0 > 0.50460704606999995, [0.053309747819196167, -0.053309747819196167], [-1.0, 1.0])
17. IF (EPInuclei_Texture_Variance_DAPIepi_3_135 > 3.9181097666300002, [-0.48063363510899532, 0.48063363510899532], [0.11151876219158123, -0.11151876219158123])
18. IF (EPInuclei_Granularity_15_DAPIepi > 10.453099637999999, [0.73079103541169688, -0.73079103541169688], [-0.11334652470683627, 0.11334652470683627])
19. IF (EPInuclei_Texture_SumEntropy_DAPIepi_3_135 > 2.5798955533800001, [-0.87789210868018597, 0.87789210868018597], [0.08076850174522561, -0.08076850174522561])
20. IF (EPInuclei_Texture_InfoMeas2_DAPIepi_3_90 > 0.85151000690199996, [0.18768806730969223, -0.18768806730969223], [-0.29504707790204499, 0.29504707790204499])
21. IF (EPInuclei_Texture_DifferenceVariance_DAPIepi_3_135 > 0.59755463059299996, [0.16913956511623879, -0.16913956511623879], [-0.38322332110407925, 0.38322332110407925])
22. IF (EPInuclei_AreaShape_Zernike_6_6 > 0.0083687884911799997, [0.11830860186917533, -0.11830860186917533], [-0.51451671596318826, 0.51451671596318826])

23. IF (EPInuclei_Granularity_11_DAPIepi > 3.4124677576, [0.26631275186995568, -0.26631275186995568], [-0.21937826989772899, 0.21937826989772899])
24. IF (EPInuclei_AreaShape_Zernike_9_9 > 0.0071875137612699997, [0.64109397561698889, -0.64109397561698889], [-0.10200362434842725, 0.10200362434842725])
25. IF (EPInuclei_Texture_AngularSecondMoment_DAPIepi_3_90 > 0.045583673469400003, [-0.069454438249420297, 0.069454438249420297], [0.73004472657310404, -0.73004472657310404])

Appendix F: ST pipeline CellProfiler™ Analyst rules

The rules listed below correspond with the cross validational accuracy graphically presented in Figure 2B. 48 postively-labeled cells and 177 negative cells were manually categorized to develop the following rules:

1. IF (STnuclei_AreaShape_Zernike_8_8 > 0.01282981029, [0.54394215087505704, -0.54394215087505704], [-0.11571486039689023, 0.11571486039689023])
2. IF (STnuclei_Granularity_3_DAPIst > 6.6728941929000003, [-0.39225678363896427, 0.39225678363896427], [0.15039716619455906, -0.15039716619455906])
3. IF (STnuclei_Intensity_UpperQuartileIntensity_DAPIst > 0.025452049449100001, [0.05916472866422974, -0.05916472866422974], [-1.0, 1.0])
4. IF (STnuclei_Texture_InfoMeas2_DAPIst_3_135 > 0.71697434339199995, [0.33758853710871145, -0.33758853710871145], [-0.16076571667256578, 0.16076571667256578])
5. IF (STnuclei_Texture_SumVariance_DAPIst_3_45 > 11.699329416199999, [-0.40238446930727778, 0.40238446930727778], [0.14542294653092697, -0.14542294653092697])
6. IF (STnuclei_AreaShape_MaximumRadius > 5.8309518948500001, [0.050545997296558738, -0.050545997296558738], [-1.0, 1.0])

7. IF (STnuclei_AreaShape_Zernike_9_5 > 0.0098639307836099997, [0.6138697500124739, -0.6138697500124739], [-0.099432960368002324, 0.099432960368002324])
8. IF (STnuclei_Texture_AngularSecondMoment_DAPIst_3_135 > 0.028730011247499999, [-0.14551235228690498, 0.14551235228690498], [0.36257553515575658, -0.36257553515575658])
9. IF (STnuclei_AreaShape_Center_Y > 873.0, [-0.71615854923277966, 0.71615854923277966], [0.072451742304032465, -0.072451742304032465])
10. IF (STnuclei_Granularity_7_DAPIst > 1.19454928918, [-0.23676470967071553, 0.23676470967071553], [0.2106270879186706, -0.2106270879186706])
11. IF (STnuclei_Texture_InfoMeas2_DAPIst_3_90 > 0.57862387876300003, [-0.081816913877562819, 0.081816913877562819], [0.60313076204694993, -0.60313076204694993])
12. IF (STnuclei_AreaShape_Zernike_6_2 > 0.0051448935765700003, [0.066728842322196877, -0.066728842322196877], [-0.88524268008176088, 0.88524268008176088])
13. IF (STnuclei_Texture_SumEntropy_DAPIst_3_90 > 2.6140335605099998, [0.39302025027760201, -0.39302025027760201], [-0.13620915792407429, 0.13620915792407429])
14. IF (STnuclei_Intensity_MADIntensity_DAPIst > 0.0056763552129300001, [-0.33591618610404733, 0.33591618610404733], [0.18233249653936545, -0.18233249653936545])

15. IF (STnuclei_Texture_Gabor_DAPIst_3 > 1.44690896515, [-0.1431015172890856, 0.1431015172890856], [0.45191133746920031, -0.45191133746920031])
16. IF (STnuclei_Texture_Correlation_DAPIst_3_135 > 0.60246974625500005, [-0.62397810415353505, 0.62397810415353505], [0.12956973695465243, -0.12956973695465243])
17. IF (STnuclei_AreaShape_Zernike_6_2 > 0.010135958107099999, [-0.21697134540916985, 0.21697134540916985], [0.24227538432719914, -0.24227538432719914])
18. IF (STnuclei_Intensity_MaxIntensity_DAPIst > 0.151934087276, [-0.90220994505031848, 0.90220994505031848], [0.0632302866513305, -0.0632302866513305])
19. IF (STnuclei_Intensity_StdIntensity_DAPIst > 0.0031431192315600001, [0.11660207933530145, -0.11660207933530145], [-0.45331892428828491, 0.45331892428828491])
20. IF (STnuclei_Texture_Variance_DAPIst_3_45 > 4.5639555555599998, [-0.61497667558537894, 0.61497667558537894], [0.10411856513753395, -0.10411856513753395])
21. IF (STnuclei_Texture_AngularSecondMoment_DAPIst_3_135 > 0.025067814539000002, [0.040564001530387611, -0.040564001530387611], [-1.0, 1.0])

22. IF (STnuclei_Intensity_IntegratedIntensity_DAPIst > 9.2263981364699994, [-0.10781929826124241, 0.10781929826124241], [0.49290086087729063, -0.49290086087729063])
23. IF (STnuclei_AreaShape_Area > 196.0, [0.0739632729924556, -0.0739632729924556], [-0.92633674774412467, 0.92633674774412467])
24. IF (STnuclei_AreaShape_Orientation > 72.449725900000004, [-0.73924543144522237, 0.73924543144522237], [0.0486324356667341, -0.0486324356667341])
25. IF (STnuclei_Intensity_MassDisplacement_DAPIst > 0.53761958689900002, [0.63541352584263222, -0.63541352584263222], [-0.083719111016634346, 0.083719111016634346])

References

1. Ginther OJ. Reproductive Biology of the Mare. 2nd ed: Equiservices; 1992.
2. Seaborn E. The oestrous cycle in the mare and some associated phenomena. The Anatomical Record. 1925;30(4):277-87.
3. Kenney RM. Cyclic and pathologic changes of the mare endometrium as detected by biopsy, with a note on early embryonic death. J Am Vet Med Assoc. 1978;172(3):241-62.
4. Ricketts SW. The Technique and Clinical Application of Endometrial Biopsy in the Mare. Equine Veterinary Journal. 1975;7(2):102-8.
5. Kenney RM, Doig PA. Equine Endometrial Biopsy, In: Current Therapy in Theriogenology. 2nd ed. Philadelphia: W. B. Saunders; 1986.
6. Snider TA, Sepoy C, Holyoak GR. Equine endometrial biopsy reviewed: observation, interpretation, and application of histopathologic data. Theriogenology. 2011;75(9):1567-81.
7. de la Concha-Bermejillo A, Kennedy PC. Prognostic value of endometrial biopsy in the mare: a retrospective analysis. J Am Vet Med Assoc. 1982;181(7):680-1.
8. Nielsen JM. Endometritis in the mare: A diagnostic study comparing cultures from swab and biopsy. Theriogenology. 2005;64(3):510-8.
9. Nielsen JM, Troedsson MH, Pedersen MR, Bojesen AM, Lehn-Jensen H, Zent WW. Diagnosis of Endometritis in the Mare Based on Bacteriological and Cytological Examinations of the Endometrium: Comparison of Results Obtained by Swabs and Biopsies. Journal of Equine Veterinary Science. 2010;30(1):27-30.
10. Ginther OJ, Pierson RA. Ultrasonic anatomy and pathology of the equine uterus. Theriogenology. 1984;21(3):505-16.
11. Hayes KE, Pierson RA, Scraba ST, Ginther OJ. Effects of estrous cycle and season on ultrasonic uterine anatomy in mares. Theriogenology. 1985;24(4):465-77.
12. Lefranc A, Allen WR. Influence of breed and oestrous cycle on endometrial gland surface density in the mare. Equine Vet J. 2007;39(6):506-10.
13. Britton BA. Endometrial change in the annual reproductive cycle of the mare. Journal of reproduction and fertility Supplement. 1982;32:175-80.
14. Watson ED, Skolnik SB, Zanecosky HG. Progesterone and estrogen receptor distribution in the endometrium of the mare. Theriogenology. 1992;38(4):575-80.
15. Aupperle H, Ozgen SHA, Schoon D, Hoppen HO, Sieme H, Tannapfel A. Cyclical endometrial steroid hormone receptor expression and proliferation intensity in the mare. Equine Vet J. 2000;32(3):228-32.
16. Lefranc A, Allen WR. Endometrial gland surface density and hyperaemia of the endometrium during early pregnancy in the mare. Equine Vet J. 2007;39(6):511-5.
17. Chavatte-Palmer P, Duchamp G, Palmer E, Ousey JC, Rossdale PD, Lombes M. Progesterone, oestrogen and glucocorticoid receptors in the uterus and mammary glands of mares from mid- to late gestation. Journal of reproduction and fertility Supplement. 2000(56):661-72.
18. Allen WR. Fetomaternal interactions and influences during equine pregnancy. Reproduction. 2001;121(4):513-27.
19. Short R. Implantation and the maternal recognition of pregnancy. Foetal Autonomy. 1969;2:31.

20. Spencer TE, Johnson GA, Burghardt RC, Bazer FW. Progesterone and placental hormone actions on the uterus: insights from domestic animals. Biol Reprod. 2004;71(1):2-10.
21. Sandra O, Constant F, Vitorino Carvalho A, Eozenou C, Valour D, Mauffre V, et al. Maternal organism and embryo biosensoring: insights from ruminants. Journal of reproductive immunology. 2015.
22. Enders AC, Liu IK. Lodgement of the equine blastocyst in the uterus from fixation through endometrial cup formation. Journal of reproduction and fertility Supplement. 1991;44:427-38.
23. McDowell KJ, Sharp DC, Grubaugh W, Thatcher WW, Wilcox CJ. Restricted conceptus mobility results in failure of pregnancy maintenance in mares. Biol Reprod. 1988;39(2):340-8.
24. Patterson AL, Squires EL, Hansen TR, Bouma GJ, Bruemmer JE. Gene profiling of inflammatory genes in day 18 endometria from pregnant and non-pregnant mares. Molecular reproduction and development. 2012;79(11):777-84.
25. Klein C, Scoggin KE, Ealy AD, Troedsson MH. Transcriptional profiling of equine endometrium during the time of maternal recognition of pregnancy. Biol Reprod. 2010;83(1):102-13.
26. Allen WR, Wilsher S. A review of implantation and early placentation in the mare. Placenta. 2009;30(12):1005-15.
27. Fiddes JC, Talmadge K. Structure, expression, and evolution of the genes for the human glycoprotein hormones. Rec Prog Hormone Res. 2013;40:43-78.
28. Pierce JG, Parsons TF. Glycoprotein hormones: structure and function. Annual review of biochemistry. 1981;50(1):465-95.
29. Noronha LE, Antczak DF. Maternal immune responses to trophoblast: the contribution of the horse to pregnancy immunology. American journal of reproductive immunology. 2010;64(4):231-44.
30. Medawar PB, editor Some immunological and endocrinological problems raised by the evolution of viviparity in vertebrates. Symp Soc Exp Biol; 1953.
31. de Mestre A, Noronha L, Wagner B, Antczak DF. Split immunological tolerance to trophoblast. The International journal of developmental biology. 2010;54(2-3):445-55.
32. Billington WD. The immunological problem of pregnancy: 50 years with the hope of progress. A tribute to Peter Medawar. Journal of reproductive immunology. 2003;60(1):1-11.
33. Donaldson WL, Zhang CH, Oriol JG, Antczak DF. Invasive equine trophoblast expresses conventional class I major histocompatibility complex antigens. Development. 1990;110(1):63-71.
34. Donaldson WL, Oriol JG, Plavin A, Antczak DF. Developmental regulation of class I major histocompatibility complex antigen expression by equine trophoblastic cells. Differentiation; research in biological diversity. 1992;52(1):69-78.
35. Maher J, Tresnan D, Deacon Sea, Hannah L, Antczak D. Analysis of MHC class I expression in equine trophoblast cells using in situ hybridization. Placenta. 1996;17(5):351-9.
36. Antczak DF, de Mestre AM, Wilsher S, Allen WR. The equine endometrial cup reaction: a fetomaternal signal of significance. Annual review of animal biosciences. 2013;1:419-42.

37. Allen WR, Stewart F. Equine placentation. Reproduction, fertility, and development. 2001;13(7-8):623-34.
38. Squires EL. Hormonal Manipulation of the Mare: A Review. Journal of Equine Veterinary Science.28(11):627-34.
39. Harrison LA, Squires EL, Nett TM, McKinnon AO. Use of gonadotropin-releasing hormone for hastening ovulation in transitional mares. J Anim Sci. 1990;68(3):690-9.
40. Brendemuehl JP, Cross DL. Influence of the dopamine antagonist domperidone on the vernal transition in seasonally anoestrous mares. Journal of reproduction and fertility Supplement. 2000(56):185-93.
41. Spencer TE, Dunlap KA, Filant J. Comparative developmental biology of the uterus: insights into mechanisms and developmental disruption. Molecular and cellular endocrinology. 2012;354(1-2):34-53.
42. Senger PL. Pathways to Pregnancy & Parturition. 3rd ed. Redmond, OR: Current Conceptions, Inc; 2012.
43. Jost A, Vigier B, Prepin J, Perchellet JP. Studies on sex differentiation in mammals. Recent progress in hormone research. 1973;29:1-41.
44. Jost A. * Recherches sur la differenciation sexuelle de lembryon de lapin 2. Action des androgenes de synthese sur l'histogenese genitale. Archives D Anatomie Microscopique et de Morphologie Experimentale. 1947;36(3):244-70.
45. Barsoum I, Yao HH. The road to maleness: from testis to Wolffian duct. Trends in endocrinology and metabolism: TEM. 2006;17(6):223-8.
46. Biason-Lauber A, Chaboissier M-C. Ovarian development and disease: The known and the unexpected. Seminars in Cell & Developmental Biology.
47. Bartol FF, Wiley AA, Bagnell CA. Uterine development and endometrial programming. Society of Reproduction and Fertility supplement. 2006;62:113-30.
48. Kobayashi A, Behringer RR. Developmental genetics of the female reproductive tract in mammals. Nature reviews Genetics. 2003;4(12):969-80.
49. Kobayashi A, Shawlot W, Kania A, Behringer RR. Requirement of Lim1 for female reproductive tract development. Development. 2004;131(3):539-49.
50. Torres M, Gomez-Pardo E, Dressler GR, Gruss P. Pax-2 controls multiple steps of urogenital development. Development. 1995;121(12):4057-65.
51. Huang CC, Orvis GD, Kwan KM, Behringer RR. Lhx1 is required in Mullerian duct epithelium for uterine development. Developmental biology. 2014;389(2):124-36.
52. Miyamoto N, Yoshida M, Kuratani S, Matsuo I, Aizawa S. Defects of urogenital development in mice lacking Emx2. Development. 1997;124(9):1653-64.
53. Miller C, Sassoon DA. Wnt-7a maintains appropriate uterine patterning during the development of the mouse female reproductive tract. Development. 1998;125(16):3201-11.
54. Biason-Lauber A, Konrad D. WNT4 and sex development. Sexual development : genetics, molecular biology, evolution, endocrinology, embryology, and pathology of sex determination and differentiation. 2008;2(4-5):210-8.
55. Carta L, Sassoon D. Wnt7a is a suppressor of cell death in the female reproductive tract and is required for postnatal and estrogen-mediated growth. Biol Reprod. 2004;71(2):444-54.

56. Franco HL, Dai D, Lee KY, Rubel CA, Roop D, Boerboom D, et al. WNT4 is a key regulator of normal postnatal uterine development and progesterone signaling during embryo implantation and decidualization in the mouse. FASEB journal : official publication of the Federation of American Societies for Experimental Biology. 2011;25(4):1176-87.
57. Hayashi K, Yoshioka S, Reardon SN, Rucker EB, 3rd, Spencer TE, DeMayo FJ, et al. WNTs in the neonatal mouse uterus: potential regulation of endometrial gland development. Biol Reprod. 2011;84(2):308-19.
58. Mericskay M, Kitajewski J, Sassoon D. Wnt5a is required for proper epithelial-mesenchymal interactions in the uterus. Development. 2004;131(9):2061-72.
59. Miller C, Pavlova A, Sassoon DA. Differential expression patterns of Wnt genes in the murine female reproductive tract during development and the estrous cycle. Mechanisms of development. 1998;76(1-2):91-9.
60. Miller RK, McCrea PD. Wnt to build a tube: contributions of Wnt signaling to epithelial tubulogenesis. Developmental dynamics : an official publication of the American Association of Anatomists. 2010;239(1):77-93.
61. Parr BA, McMahon AP. Sexually dimorphic development of the mammalian reproductive tract requires Wnt-7a. Nature. 1998;395(6703):707-10.
62. Sassoon D. Wnt genes and endocrine disruption of the female reproductive tract: a genetic approach. Molecular and cellular endocrinology. 1999;158(1-2):1-5.
63. Deutscher E, Hung-Chang Yao H. Essential roles of mesenchyme-derived beta-catenin in mouse Mullerian duct morphogenesis. Developmental biology. 2007;307(2):227-36.
64. Taylor HS, Vanden Heuvel GB, Igarashi P. A conserved Hox axis in the mouse and human female reproductive system: late establishment and persistent adult expression of the Hoxa cluster genes. Biol Reprod. 1997;57(6):1338-45.
65. Mark M, Rijli FM, Chambon P. Homeobox genes in embryogenesis and pathogenesis. Pediatric research. 1997;42(4):421-9.
66. Wilsher S, Lefranc AC, Allen WR. Post natal oestrogen administration stimulates precocious endometrial gland development in the horse. Equine Vet J. 2009;41(7):678-84.
67. Gerstenberg C, Allen WR. Development of equine endometrial glands from fetal life to ovarian cyclicity. Journal of reproduction and fertility Supplement. 2000(56):317-26.
68. Bartol FF, Wiley AA, Floyd JG, Ott TL, Bazer FW, Gray CA, et al. Uterine differentiation as a foundation for subsequent fertility. Journal of reproduction and fertility Supplement. 1999;54:287-302.
69. Bartol FF, Wiley AA, Spencer TE, Vallet JL, Christenson RK. Early uterine development in pigs. Journal of reproduction and fertility Supplement. 1993;48:99-116.
70. Gray CA, Bartol FF, Tarleton BJ, Wiley AA, Johnson GA, Bazer FW, et al. Developmental biology of uterine glands. Biol Reprod. 2001;65(5):1311-23.
71. Masters RA, Crean BD, Yan W, Moss AG, Ryan PL, Wiley AA, et al. Neonatal porcine endometrial development and epithelial proliferation affected by age and exposure to estrogen and relaxin. Domestic animal endocrinology. 2007;33(3):335-46.

72. Cooke PS, Spencer TE, Bartol FF, Hayashi K. Uterine glands: development, function and experimental model systems. Molecular human reproduction. 2013;19(9):547-58.
73. Cooke PS, Borsdorf DC, Ekman GC, Doty KF, Clark SG, Dziuk PJ, et al. Uterine gland development begins postnatally and is accompanied by estrogen and progesterone receptor expression in the dog. Theriogenology. 2012;78(8):1787-95.
74. Cooke PS, Ekman GC, Kaur J, Davila J, Bagchi IC, Clark SG, et al. Brief exposure to progesterone during a critical neonatal window prevents uterine gland formation in mice. Biol Reprod. 2012;86(3):63.
75. Bartol FF, Bagnell CA. Lactocrine programming of female reproductive tract development: environmental connections to the reproductive continuum. Molecular and cellular endocrinology. 2012;354(1-2):16-21.
76. Bartol FF, Wiley AA, Miller DJ, Silva AJ, Roberts KE, Davolt ML, et al. Lactation Biology Symposium: lactocrine signaling and developmental programming. J Anim Sci. 2013;91(2):696-705.
77. Spencer TE, Gray CA. Sheep uterine gland knockout (UGKO) model. Methods in molecular medicine. 2006;121:85-94.
78. Tarleton BJ, Wiley AA, Bartol FF. Endometrial development and adenogenesis in the neonatal pig: effects of estradiol valerate and the antiestrogen ICI 182,780. Biol Reprod. 1999;61(1):253-63.
79. Spencer TE. Hormonal manipulation of endometrial gland development in the horse. Equine Vet J. 2009;41(7):617-8.
80. Gray CA, Bartol FF, Taylor KM, Wiley AA, Ramsey WS, Ott TL, et al. Ovine uterine gland knock-out model: effects of gland ablation on the estrous cycle. Biol Reprod. 2000;62(2):448-56.
81. Gray CA, Burghardt RC, Johnson GA, Bazer FW, Spencer TE. Evidence that absence of endometrial gland secretions in uterine gland knockout ewes compromises conceptus survival and elongation. Reproduction. 2002;124(2):289-300.
82. Bartol FF, Johnson LL, Floyd JG, Wiley AA, Spencer TE, Buxton DF, et al. Neonatal exposure to progesterone and estradiol alters uterine morphology and luminal protein content in adult beef heifers. Theriogenology. 1995;43(5):835-44.
83. Bartol FF, Wiley AA, Coleman DA, Wolfe DF, Riddell MG. Ovine uterine morphogenesis: effects of age and progestin administration and withdrawal on neonatal endometrial development and DNA synthesis. J Anim Sci. 1988;66(11):3000-9.
84. RR W, AA W, KI B, AK J, NS F, GA D, et al., editors. Neonatal exposure to medroxyprogesterone acetate alters canine uterine development The Society for Theriogenology Annual Conference; 2014; Portland, OR, USA.
85. Ponchon T, Lopez Merlo M, Faya M, Priotto M, Barbeito C, Gobello C. Postnatal exposure to a progestin does not prevent uterine adenogenesis in domestic dogs. Journal of veterinary science. 2015.
86. Dhakal P, Rumi MA, Kubota K, Chakraborty D, Chien J, Roby KF, et al. Neonatal Progesterone Programs Adult Uterine Responses to Progesterone and Susceptibility to Uterine Dysfunction. Endocrinology. 2015;156(10):3791-803.
87. Miller DJ, Wiley AA, Chen JC, Bagnell CA, Bartol FF. Nursing for 48 hours from birth supports porcine uterine gland development and endometrial cell compartment-specific gene expression. Biol Reprod. 2013;88(1):4.

88. Chen JC, Frankshun AL, Wiley AA, Miller DJ, Welch KA, Ho TY, et al. Milk-borne lactocrine-acting factors affect gene expression patterns in the developing neonatal porcine uterus. Reproduction. 2011;141(5):675-83.
89. Frankshun AL, Chen J, Barron LA, Ho TY, Miller DJ, Rahman KM, et al. Nursing during the first two days of life is essential for the expression of proteins important for growth and remodeling of the neonatal porcine cervix. Endocrinology. 2012;153(9):4511-21.
90. Vallet JL, Miles JR, Rempel LA, Nonneman DJ, Lents CA. Relationships between day one piglet serum immunoglobulin immunocrit and subsequent growth, puberty attainment, litter size, and lactation performance. J Anim Sci. 2015;93(6):2722-9.
91. Overview of Immunohistochemistry: Life Technologies; [3/24/15]. Available from: https://www.lifetechnologies.com/us/en/home/life-science/protein-biology/protein-biology-learning-center/protein-biology-resource-library/pierce-protein-methods/overview-immunohistochemistry.html.
92. Mylonas I, Makovitzky J, Friese K, Jeschke U. Immunohistochemical labelling of steroid receptors in normal and malignant human endometrium. Acta histochemica. 2009;111(4):349-59.
93. D'Angelo E, Prat J. Diagnostic use of immunohistochemistry in uterine mesenchymal tumors. Seminars in diagnostic pathology. 2014;31(3):216-22.
94. Deavers MT, Malpica A, Silva EG. Immunohistochemistry in gynecological pathology. International journal of gynecological cancer : official journal of the International Gynecological Cancer Society. 2003;13(5):567-79.
95. Giordano G. Value of immunohistochemistry in uterine pathology: common and rare diagnostic dilemmas. Pathology, research and practice. 2009;205(10):663-76.
96. Kaspar HG, Crum CP. The utility of immunohistochemistry in the differential diagnosis of gynecologic disorders. Archives of pathology & laboratory medicine. 2015;139(1):39-54.
97. McCluggage WG. Recent advances in immunohistochemistry in gynaecological pathology. Histopathology. 2002;40(4):309-26.
98. Hartt LS, Carling SJ, Joyce MM, Johnson GA, Vanderwall DK, Ott TL. Temporal and spatial associations of oestrogen receptor alpha and progesterone receptor in the endometrium of cyclic and early pregnant mares. Reproduction. 2005;130(2):241-50.
99. Wilsher S, Gower S, Allen WR. Immunohistochemical localisation of progesterone and oestrogen receptors at the placental interface in mares during early pregnancy. Animal reproduction science. 2011;129(3-4):200-8.
100. Antibodies: A Laboratory Manual. 2nd ed: John Inglis; 2014.
101. Howat WJ, Wilson BA. Tissue fixation and the effect of molecular fixatives on downstream staining procedures. Methods. 2014;70(1):12-9.
102. Fox CH, Johnson FB, Whiting J, Roller PP. Formaldehyde fixation. Journal of Histochemistry & Cytochemistry. 1985;33(8):845-53.
103. Rait VK, Xu L, O'Leary TJ, Mason JT. Modeling formalin fixation and antigen retrieval with bovine pancreatic RNase A II. Interrelationship of cross-linking, immunoreactivity, and heat treatment. Laboratory investigation; a journal of technical methods and pathology. 2004;84(3):300-6.
104. Shi SR, Key ME, Kalra KL. Antigen retrieval in formalin-fixed, paraffin-embedded tissues: an enhancement method for immunohistochemical staining based on

microwave oven heating of tissue sections. Journal of Histochemistry & Cytochemistry. 1991;39(6):741-8.
105. Vincek V, Nassiri M, Nadji M, Morales AR. A tissue fixative that protects macromolecules (DNA, RNA, and protein) and histomorphology in clinical samples. Laboratory investigation; a journal of technical methods and pathology. 2003;83(10):1427-35.
106. Turashvili G, Yang W, McKinney S, Kalloger S, Gale N, Ng Y, et al. Nucleic acid quantity and quality from paraffin blocks: Defining optimal fixation, processing and DNA/RNA extraction techniques. Experimental and Molecular Pathology. 2012;92(1):33-43.
107. Steu S, Baucamp M, von Dach G, Bawohl M, Dettwiler S, Storz M, et al. A procedure for tissue freezing and processing applicable to both intra-operative frozen section diagnosis and tissue banking in surgical pathology. Virchows Archiv : an international journal of pathology. 2008;452(3):305-12.
108. Weston LA, Hummon AB. Comparative LC-MS/MS analysis of optimal cutting temperature (OCT) compound removal for the study of mammalian proteomes. The Analyst. 2013;138(21):6380-4.
109. Loken SD, Demetrick DJ. A novel method for freezing and storing research tissue bank specimens. Human pathology. 2005;36(9):977-80.
110. Daneshtalab N, Dore JJ, Smeda JS. Troubleshooting tissue specificity and antibody selection: Procedures in immunohistochemical studies. Journal of pharmacological and toxicological methods. 2010;61(2):127-35.
111. Otali D, Stockard CR, Oelschlager DK, Wan W, Manne U, Watts SA, et al. Combined effects of formalin fixation and tissue processing on immunorecognition. Biotechnic & histochemistry : official publication of the Biological Stain Commission. 2009;84(5):223-47.
112. Leenaars PP, Hendriksen CF, de Leeuw WA, Carat F, Delahaut P, Fischer R, et al. The Production of Polyclonal Antibodies in Laboratory Animals. The Report and Recommendations of ECVAM Workshop 35. Alternatives to laboratory animals : ATLA. 1999;27(1):79-102.
113. Lipman NS, Jackson LR, Trudel LJ, Weis-Garcia F. Monoclonal versus polyclonal antibodies: distinguishing characteristics, applications, and information resources. ILAR journal / National Research Council, Institute of Laboratory Animal Resources. 2005;46(3):258-68.
114. van der Loos CM. Multiple immunoenzyme staining: methods and visualizations for the observation with spectral imaging. The journal of histochemistry and cytochemistry : official journal of the Histochemistry Society. 2008;56(4):313-28.
115. Mansfield JR, Hoyt C, Levenson RM. Visualization of microscopy-based spectral imaging data from multi-label tissue sections. Current protocols in molecular biology / edited by Frederick M Ausubel [et al]. 2008;Chapter 14:Unit 14.9.
116. User's Manual for Nuance 2.10. Woburn, MA: Cambridge Research & Instrumentation, Inc; 2009.
117. Neher R, Neher E. Optimizing imaging parameters for the separation of multiple labels in a fluorescence image. Journal of microscopy. 2004;213(Pt 1):46-62.
118. Levenson RM, Mansfield JR. Multispectral imaging in biology and medicine: slices of life. Cytometry part A. 2006;69(8):748-58.

119. Gronemeyer H, Gustafsson JA, Laudet V. Principles for modulation of the nuclear receptor superfamily. Nature reviews Drug discovery. 2004;3(11):950-64.
120. Eick GN, Colucci JK, Harms MJ, Ortlund EA, Thornton JW. Evolution of minimal specificity and promiscuity in steroid hormone receptors. PLoS genetics. 2012;8(11):e1003072.
121. Katzenellenbogen JA. The structural pervasiveness of estrogenic activity. Environmental health perspectives. 1995;103 Suppl 7:99-101.
122. Lathe R, Kotelevtsev Y. Steroid signaling: ligand-binding promiscuity, molecular symmetry, and the need for gating. Steroids. 2014;82:14-22.
123. Leonhardt SA, Boonyaratanakornkit V, Edwards DP. Progesterone receptor transcription and non-transcription signaling mechanisms. Steroids. 2003;68(10-13):761-70.
124. Cato ACB, Nestl A, Mink S. Rapid Actions of Steroid Receptors in Cellular Signaling Pathways. Science Signaling. 2002;2002(138):re9-re.
125. Hache RJ, Tse R, Reich T, Savory JG, Lefebvre YA. Nucleocytoplasmic trafficking of steroid-free glucocorticoid receptor. The Journal of biological chemistry. 1999;274(3):1432-9.
126. Vandevyver S, Dejager L, Libert C. On the trail of the glucocorticoid receptor: into the nucleus and back. Traffic (Copenhagen, Denmark). 2012;13(3):364-74.
127. Vandevyver S, Dejager L, Libert C. Comprehensive overview of the structure and regulation of the glucocorticoid receptor. Endocr Rev. 2014;35(4):671-93.
128. Pratt WB, Toft DO. Steroid receptor interactions with heat shock protein and immunophilin chaperones. Endocr Rev. 1997;18(3):306-60.
129. Barnes PJ. Anti-inflammatory actions of glucocorticoids: molecular mechanisms. Clinical science. 1998;94(6):557-72.
130. Falkenstein E, Tillmann HC, Christ M, Feuring M, Wehling M. Multiple actions of steroid hormones--a focus on rapid, nongenomic effects. Pharmacological reviews. 2000;52(4):513-56.
131. Nemere I, Farach-Carson MC. Membrane receptors for steroid hormones: a case for specific cell surface binding sites for vitamin D metabolites and estrogens. Biochemical and biophysical research communications. 1998;248(3):443-9.
132. Simoncini T, Mannella P, Fornari L, Caruso A, Varone G, Genazzani AR. Genomic and non-genomic effects of estrogens on endothelial cells. Steroids. 2004;69(8-9):537-42.
133. Ascenzi P, Bocedi A, Marino M. Structure-function relationship of estrogen receptor alpha and beta: impact on human health. Molecular aspects of medicine. 2006;27(4):299-402.
134. Filardo EJ, Thomas P. Minireview: G protein-coupled estrogen receptor-1, GPER-1: its mechanism of action and role in female reproductive cancer, renal and vascular physiology. Endocrinology. 2012;153(7):2953-62.
135. Maggiolini M, Picard D. The unfolding stories of GPR30, a new membrane-bound estrogen receptor. The Journal of endocrinology. 2010;204(2):105-14.
136. Jordan VC. Antiestrogens and selective estrogen receptor modulators as multifunctional medicines. 1. Receptor interactions. Journal of medicinal chemistry. 2003;46(6):883-908.

137. Jordan VC. Antiestrogens and selective estrogen receptor modulators as multifunctional medicines. 2. Clinical considerations and new agents. Journal of medicinal chemistry. 2003;46(7):1081-111.
138. Pearce ST, Jordan VC. The biological role of estrogen receptors α and β in cancer. Critical reviews in oncology/hematology. 2004;50(1):3-22.
139. Deroo BJ, Korach KS. Estrogen receptors and human disease. The Journal of clinical investigation. 2006;116(3):561.
140. Tibbetts TA, Mendoza-Meneses M, O'Malley BW, Conneely OM. Mutual and intercompartmental regulation of estrogen receptor and progesterone receptor expression in the mouse uterus. Biol Reprod. 1998;59(5):1143-52.
141. Lubahn DB, Moyer JS, Golding TS, Couse JF, Korach KS, Smithies O. Alteration of reproductive function but not prenatal sexual development after insertional disruption of the mouse estrogen receptor gene. Proceedings of the National Academy of Sciences of the United States of America. 1993;90(23):11162-6.
142. Korach KS. Insights from the study of animals lacking functional estrogen receptor. Science. 1994;266(5190):1524-7.
143. Lear TL, Adams MH, Sullivan ND, McDowell KJ, Bailey E. Assignment of the horse progesterone receptor (PGR) and estrogen receptor (ESR1) genes to horse chromosomes 7 and 31, respectively, by in situ hybridization. Cytogenetics and cell genetics. 1998;82(1-2):110-1.
144. Weihua Z, Saji S, Makinen S, Cheng G, Jensen EV, Warner M, et al. Estrogen receptor (ER) beta, a modulator of ERalpha in the uterus. Proceedings of the National Academy of Sciences of the United States of America. 2000;97(11):5936-41.
145. Brandenberger AW, Tee MK, Lee JY, Chao V, Jaffe RB. Tissue distribution of estrogen receptors alpha (ER-alpha) and beta (ER-beta) mRNA in the midgestational human fetus. The Journal of clinical endocrinology and metabolism. 1997;82(10):3509-12.
146. Bigsby RM. Control of growth and differentiation of the endometrium: the role of tissue interactions. Annals of the New York Academy of Sciences. 2002;955:110-7; discussion 8, 396-406.
147. Cooke P, Buchanan D, Young P, Setiawan T, Brody J, Korach K, et al. Stromal estrogen receptors mediate mitogenic effects of estradiol on uterine epithelium. Proceedings of the National Academy of Sciences. 1997;94(12):6535-40.
148. Conneely OM, Mulac-Jericevic B, Lydon JP. Progesterone-dependent regulation of female reproductive activity by two distinct progesterone receptor isoforms. Steroids. 2003;68(10-13):771-8.
149. Evans RM. The steroid and thyroid hormone receptor superfamily. Science. 1988;240(4854):889-95.
150. Tsai MJ, O'Malley BW. Molecular mechanisms of action of steroid/thyroid receptor superfamily members. Annual review of biochemistry. 1994;63:451-86.
151. Graham JD, Clarke CL. Physiological Action of Progesterone in Target Tissues 1. Endocrine reviews. 1997;18(4):502-19.
152. Kastner P, Krust A, Turcotte B, Stropp U, Tora L, Gronemeyer H, et al. Two distinct estrogen-regulated promoters generate transcripts encoding the two functionally different human progesterone receptor forms A and B. The EMBO journal. 1990;9(5):1603-14.

153. Wen DX, Xu YF, Mais DE, Goldman ME, McDonnell DP. The A and B isoforms of the human progesterone receptor operate through distinct signaling pathways within target cells. Molecular and cellular biology. 1994;14(12):8356-64.
154. McDonnell DP, Shahbaz MM, Vegeto E, Goldman ME. The human progesterone receptor A-form functions as a transcriptional modulator of mineralocorticoid receptor transcriptional activity. The Journal of steroid biochemistry and molecular biology. 1994;48(5-6):425-32.
155. Boonyaratanakornkit V, Scott MP, Ribon V, Sherman L, Anderson SM, Maller JL, et al. Progesterone receptor contains a proline-rich motif that directly interacts with SH3 domains and activates c-Src family tyrosine kinases. Molecular cell. 2001;8(2):269-80.
156. Conneely OM, Lydon JP. Progesterone receptors in reproduction: functional impact of the A and B isoforms. Steroids. 2000;65(10-11):571-7.
157. Moussatche P, Lyons T. Non-genomic progesterone signalling and its non-canonical receptor. Biochemical Society transactions. 2012;40(1):200.
158. Lydon JP, DeMayo FJ, Funk CR, Mani SK, Hughes AR, Montgomery CA, Jr., et al. Mice lacking progesterone receptor exhibit pleiotropic reproductive abnormalities. Genes & development. 1995;9(18):2266-78.
159. Mani SK, Allen JM, Lydon JP, Mulac-Jericevic B, Blaustein JD, DeMayo FJ, et al. Dopamine requires the unoccupied progesterone receptor to induce sexual behavior in mice. Molecular endocrinology (Baltimore, Md). 1996;10(12):1728-37.
160. Chappell PE, Schneider JS, Kim P, Xu M, Lydon JP, O'Malley BW, et al. Absence of gonadotropin surges and gonadotropin-releasing hormone self-priming in ovariectomized (OVX), estrogen (E2)-treated, progesterone receptor knockout (PRKO) mice. Endocrinology. 1999;140(8):3653-8.
161. Tibbetts TA, DeMayo F, Rich S, Conneely OM, O'Malley BW. Progesterone receptors in the thymus are required for thymic involution during pregnancy and for normal fertility. Proceedings of the National Academy of Sciences of the United States of America. 1999;96(21):12021-6.
162. Clarke CL, Sutherland RL. Progestin regulation of cellular proliferation. Endocr Rev. 1990;11(2):266-301.
163. Bigsby RM, Cunha GR. Effects of progestins and glucocorticoids on deoxyribonucleic acid synthesis in the uterus of the neonatal mouse. Endocrinology. 1985;117(6):2520-6.
164. Zhou J, Cidlowski JA. The human glucocorticoid receptor: one gene, multiple proteins and diverse responses. Steroids. 2005;70(5-7):407-17.
165. Schmid W, Cole TJ, Blendy JA, Schutz G. Molecular genetic analysis of glucocorticoid signalling in development. The Journal of steroid biochemistry and molecular biology. 1995;53(1-6):33-5.
166. Beato M, Klug J. Steroid hormone receptors: an update. Human reproduction update. 2000;6(3):225-36.
167. Cole TJ, Blendy JA, Monaghan AP, Krieglstein K, Schmid W, Aguzzi A, et al. Targeted disruption of the glucocorticoid receptor gene blocks adrenergic chromaffin cell development and severely retards lung maturation. Genes & development. 1995;9(13):1608-21.

168. Ballard PL, Baxter JD, Higgins SJ, Rousseau GG, Tomkins GM. General presence of glucocorticoid receptors in mammalian tissues. Endocrinology. 1974;94(4):998-1002.
169. Velardo JT, Hisaw FL, Bever AT. Inhibitory action of desoxycorticosterone acetate, cortisone acetate, and testosterone on uterine growth induced by estradiol-17β 1. Endocrinology. 1956;59(2):165-9.
170. Rhen T, Grissom S, Afshari C, Cidlowski JA. Dexamethasone blocks the rapid biological effects of 17beta-estradiol in the rat uterus without antagonizing its global genomic actions. FASEB journal : official publication of the Federation of American Societies for Experimental Biology. 2003;17(13):1849-70.
171. Nanjappa MK, Medrano TI, Lydon JP, Bigsby RM, Cooke PS. Maximal Dexamethasone Inhibition of Luminal Epithelial Proliferation Involves Progesterone Receptor (PR)- and Non-PR-Mediated Mechanisms in Neonatal Mouse Uterus. Biol Reprod. 2015;92(5):122.
172. Bamberger AM, Milde-Langosch K, Loning T, Bamberger CM. The glucocorticoid receptor is specifically expressed in the stromal compartment of the human endometrium. The Journal of clinical endocrinology and metabolism. 2001;86(10):5071-4.
173. Gerdes J, Lemke H, Baisch H, Wacker HH, Schwab U, Stein H. Cell cycle analysis of a cell proliferation-associated human nuclear antigen defined by the monoclonal antibody Ki-67. Journal of immunology. 1984;133(4):1710-5.
174. Schluter C, Duchrow M, Wohlenberg C, Becker MH, Key G, Flad HD, et al. The cell proliferation-associated antigen of antibody Ki-67: a very large, ubiquitous nuclear protein with numerous repeated elements, representing a new kind of cell cycle-maintaining proteins. The Journal of cell biology. 1993;123(3):513-22.
175. Duchrow M, Schluter C, Wohlenberg C, Flad HD, Gerdes J. Molecular characterization of the gene locus of the human cell proliferation-associated nuclear protein defined by monoclonal antibody Ki-67. Cell proliferation. 1996;29(1):1-12.
176. van Dierendonck JH, Keijzer R, van de Velde CJ, Cornelisse CJ. Nuclear distribution of the Ki-67 antigen during the cell cycle: comparison with growth fraction in human breast cancer cells. Cancer research. 1989;49(11):2999-3006.
177. Scholzen T, Gerdes J. The Ki-67 protein: from the known and the unknown. Journal of cellular physiology. 2000;182(3):311-22.
178. van Oijen MG, Medema RH, Slootweg PJ, Rijksen G. Positivity of the proliferation marker Ki-67 in noncycling cells. American journal of clinical pathology. 1998;110(1):24-31.
179. Gerdes J, Dallenbach F, Lennert K, Lemke H, Stein H. Growth fractions in malignant non-Hodgkin's lymphomas (NHL) as determined in situ with the monoclonal antibody Ki-67. Hematological oncology. 1984;2(4):365-71.
180. Grogan TM, Lippman SM, Spier CM, Slymen DJ, Rybski JA, Rangel CS, et al. Independent prognostic significance of a nuclear proliferation antigen in diffuse large cell lymphomas as determined by the monoclonal antibody Ki-67. Blood. 1988;71(4):1157-60.
181. Hall PA, Richards MA, Gregory WM, d'Ardenne AJ, Lister TA, Stansfeld AG. The prognostic value of Ki67 immunostaining in non-Hodgkin's lymphoma. The Journal of pathology. 1988;154(3):223-35.

182. Bouzubar N, Walker KJ, Griffiths K, Ellis IO, Elston CW, Robertson JF, et al. Ki67 immunostaining in primary breast cancer: pathological and clinical associations. British journal of cancer. 1989;59(6):943-7.
183. Holte H, de Lange Davies C, Beiske K, Stokke T, Marton PF, Smeland EB, et al. Ki67 and 4F2 antigen expression as well as DNA synthesis predict survival at relapse/tumour progression in low-grade B-cell lymphoma. International journal of cancer Journal international du cancer. 1989;44(6):975-80.
184. Nicholson RI, Bouzubar N, Walker KJ, McClelland R, Dixon AR, Robertson JF, et al. Hormone sensitivity in breast cancer: influence of heterogeneity of oestrogen receptor expression and cell proliferation. European journal of cancer. 1991;27(7):908-13.
185. Tungekar MF, Gatter KC, Dunnill MS, Mason DY. Ki-67 immunostaining and survival in operable lung cancer. Histopathology. 1991;19(6):545-50.
186. Wintzer HO, Zipfel I, Schulte-Mönting J, Hellerich U, von Kleist S. Ki-67 immunostaining in human breast tumors and its relationship to prognosis. Cancer. 1991;67(2):421-8.
187. Fontana D, Bellina M, Gubetta L, Fasolis G, Rolle L, Scoffone C, et al. Monoclonal antibody Ki-67 in the study of the proliferative activity of bladder carcinoma. The Journal of urology. 1992;148(4):1149-51.
188. Prosperi E. Multiple roles of the proliferating cell nuclear antigen: DNA replication, repair and cell cycle control. Progress in cell cycle research. 1997;3:193-210.
189. Miyachi K, Fritzler MJ, Tan EM. Autoantibody to a nuclear antigen in proliferating cells. Journal of immunology. 1978;121(6):2228-34.
190. Stockard CR. Developmental rate and structural expression: An experimental study of twins, ‘double monsters’ and single deformities and the interaction among embryoninc organs during their origin and development. The American journal of anatomy. 1921:115.
191. Barker DJ. The fetal and infant origins of adult disease. Bmj. 1990;301(6761):1111-.
192. al Saati T, Clamens S, Cohen-Knafo E, Faye JC, Prats H, Coindre JM, et al. Production of monoclonal antibodies to human estrogen-receptor protein (ER) using recombinant ER (RER). International journal of cancer Journal international du cancer. 1993;55(4):651-4.
193. Kumar V, Green S, Stack G, Berry M, Jin JR, Chambon P. Functional domains of the human estrogen receptor. Cell. 1987;51(6):941-51.
194. Traish AM, Wotiz HH. Monoclonal and polyclonal antibodies to human progesterone receptor peptide-(533-547) recognize a specific site in unactivated (8S) and activated (4S) progesterone receptor and distinguish between intact and proteolyzed receptors. Endocrinology. 1990;127(3):1167-75.
195. Wiley AA, Bartol FF, Barron DH. Histogenesis of the ovine uterus. J Anim Sci. 1987;64(4):1262-9.
196. Atkinson BA, King GJ, Amoroso EC. Development of the caruncular and intercaruncular regions in the bovine endometrium. Biol Reprod. 1984;30(3):763-74.
197. Valdes-Dapena M. The development of the uterus in late fetal life, infancy, and childhood. The Uterus (International Academy of Pathology Monograph Series) Melbourne, FL: Krieger Pub Co. 1973:40-67.

198. Rider V. Progesterone and the control of uterine cell proliferation and differentiation. Frontiers in bioscience : a journal and virtual library. 2002;7:d1545-55.
199. Vicent GP, Ballare C, Zaurin R, Saragueta P, Beato M. Chromatin remodeling and control of cell proliferation by progestins via cross talk of progesterone receptor with the estrogen receptors and kinase signaling pathways. Annals of the New York Academy of Sciences. 2006;1089:59-72.
200. Dressing GE, Lange CA. Integrated actions of progesterone receptor and cell cycle machinery regulate breast cancer cell proliferation. Steroids. 2009;74(7):573-6.
201. Dickmeis T, Foulkes NS. Glucocorticoids and circadian clock control of cell proliferation: at the interface between three dynamic systems. Molecular and cellular endocrinology. 2011;331(1):11-22.
202. Nakai R, Weng Q, Tanaka Y, TSUNODA N, TANIYAMA H, HARAMAKI S, et al. Change in Circulating Follicle-Stimulating Hormone, Luteinizing Hormone, Immunoreactive Inhibin, Progesterone, Testosterone and Estradiol-17. BETA. in Fillies from Birth to 6 Months of Age. Journal of Equine Science. 2007;18(3):85-91.